Remote Sens. **2013**, *5*, 1651-1680; doi:10.3390/rs5041651

OPEN ACCESS

Remote Sensing

ISSN 2072-4292

www.mdpi.com/journal/remotesensing

Article

Water Balance Modeling in a Semi-Arid Environment with Limited *in situ* Data Using Remote Sensing in Lake Manyara, East African Rift, Tanzania

Dorothea Deus [1,2,*], Richard Gloaguen [1,3] and Peter Krause [4]

[1] Remote Sensing Group, Institute of Geology, Faculty of Geosciences, Geoengineering and Mining, Freiberg University of Mining and Technology (TUBAF), Bernhard-von-Cotta Str. 2, D-09596 Freiberg, Germany; E-Mail: gloaguen@geo.tu-freiberg.de

[2] Department of Geomatics, School of Geospatial Sciences and Technology (SGST), Ardhi University, Dar es Salaam, Tanzania

[3] Remote Sensing Group, Helmholtz Institute Freiberg of Resource Technology, Halsbrueckerstr. 34, D-09599 Freiberg, Germany; E-Mail: r.gloaguen@hzdr.de

[4] Thüringer Landesanstalt für Umwelt und Geologie (TLUG), Abteilung 5–Wasserwirtschaft–Referat 51. Gewässerkundlicher Landesdienst, Hochwassernachrichtenzentrale. Göschwitzer Str. 41, D-07745 Jena; E-Mail: peter.krause@tlug.thueringen.de

***** Author to whom correspondence should be addressed; E-Mail: dorothd@gmail.com; Tel.: +49-373-139-2806; Fax: +49-373-139-3599.

Received: 7 February 2013; in revised form: 22 March 2013 / Accepted: 26 March 2013 / Published: 2 April 2013

Abstract: The purpose of this paper is to estimate the water balance in a semi-arid environment with limited *in situ* data using a remote sensing approach. We focus on the Lake Manyara catchment, located within the East African Rift of northern Tanzania. We use a distributed conceptual hydrological model driven by remote sensing data to study the spatial and temporal variability of water balance parameters within the catchment. Satellite gravimetry GRACE data is used to verify the trends of the inferred lake level changes. The results show that the lake undergoes high spatial and temporal variations, characteristic of a semi-arid climate with high evaporation and low rainfall. We observe that the Lake Manyara water balance and GRACE equivalent water depth show comparable trends; a decrease after 2002 followed by a sharp increase in 2006–2007. Our modeling confirms the importance of the 2006–2007 Indian Ocean Dipole fluctuation in replenishing the groundwater reservoirs of East Africa. We thus demonstrate that water balance modeling can be performed successfully using remote sensing data even in complex climatic settings.

Despite the small size of Lake Manyara, GRACE data showed great potential for hydrological research on smaller un-gauged lakes and catchments in similar semi-arid environments worldwide. The water balance information can be used for further analysis of lake variations in relation to soil erosion, climate and land cover/land use change as well as different lake management and conservation scenarios.

Keywords: semi-arid; water balance; remote sensing; rainfall; evapotranspiration; runoff; GRACE

1. Introduction

We investigate the water balance for a lake and its catchment, located in a semi-arid hydrological setting using a hydrological model driven by remote sensing data. Quantifying the hydrological budget in arid and semi-arid regions is important as the scarcity of water and climatic variability lead to conflicts related to water use [1,2]. Water resources in semi-arid regions have received slight consideration principally due to their complexity and a lack of *in situ* data [3]. However, the advent of satellite derived hydro-meteorological measurements and increased stress on water resources has triggered more interest in such research [1,3]. The hydrological dynamics of a semi-arid catchment basin as expressed by both direct and base flow is affected by a number of factors including the spatial variation of topography, soils, vegetation, land use, river topography, structural geology and the spatial temporal variation of climate [4]. In many semi-arid regions of the world surface reservoirs provide the major source of water [2].

Lakes are dynamic entities, sensitive to climatic and environmental changes. In the East African Rift, the topography of the rift escarpments and volcanic highlands plays an important role in controlling local climate and thus the lake basins [5–7]. Thus, lakes are sensitive indicators of changes in the balance between precipitation, water flow into the lake, and water loss from the lake through evaporation, seepage and drainage. Lake Manyara is an example of a lake that has fluctuated considerably in depth and area over recent years [8]. On the other hand, an estimate of Lake Manyara's water balance is difficult as the largest part of its catchment is un-gauged and the inflow is unknown.

In this study, we use remote sensing (RS) observations to approximate the spatial and temporal variation of hydrological parameters over lake Manyara and its catchment, which are used as inputs for the J2000g, a distributed conceptual hydrological model [9]. Some ground measurement and satellite gravimetry derived equivalent water thickness has been employed to verify the trend of the Lake Manyara water balance [10]. Over recent years, several studies have both applied remote sensing observations and gravimetry recovery and climate experiment (GRACE) measurements to study the hydrological cycles of lakes, rivers and associated basins in the East African Rift and elsewhere [10–15]. Changes in a basin's water budget are directly linked to local gravity variations [16]. GRACE derived terrestrial water storage (TWS) variation can be considered as a proxy of the global water cycle as it reflects changes soil water storage, snow over land, and groundwater reservoirs. The TWS is closely associated to the components of water balance (*i.e.*, accumulated precipitation (P), evapotranspiration (ET), surface and water storage) within a given catchment or area [12]. Despite the problem related to

GRACE's coarse spatial resolution, we make use of the dataset in this research due to its the strong hydrological signal over the selected study area [17].

The purpose of this work is to utilize remote sensing dataset with spatial resolution ranging from 0.05 to 1 degree with the following objectives: (a) to quantify the water balance components in the lake and the overall basin; (b) to test the applicability of the J2000g hydrological model in a data poor semi-arid lake basin; and to (c) test the usability of GRACE satellite gravimetry total water storage (TWS) data on small un-gauged lake catchment basins and minor lakes that are not included in the global satellite altimetry mission network.

2. Description of the Study Area

2.1. Setting

Lake Manyara is the southernmost lake within the eastern arm of the Gregory Rift Valley System and is characterized by widespread volcanicity [5,8]. The Quaternary rifting and volcanism still exerts a strong control on surface morphology [18–20]. The shallow and saline lake is located about 126 km west of Arusha, Northern Tanzania (3 °25'–3 °48'S, 35 °44'–35 °53'E, 960 m a.s.l., Figure 1).

Figure 1. Lake Manyara and its catchment basin in northern Tanzania.

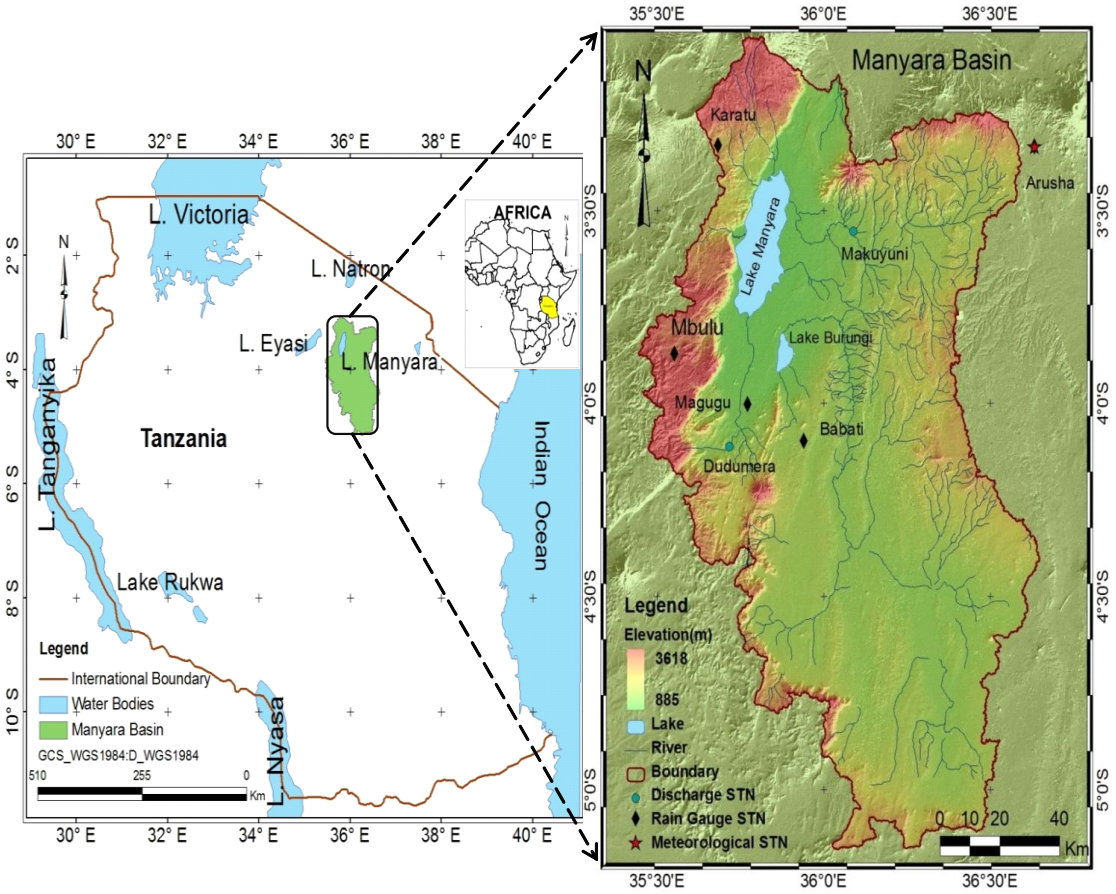

The lake varies from 410 to 480 km^2 in area and has dried up completely at certain times [5]. The present Lake Manyara is the residual portion of a much larger palaeolake that was 300 meters deeper. Somi [21] reconstructed Lake Manyara palaeo-shorelines based on evidence from shore marks, algal

stromatolites and beach deposits. A May/June 2010 bathymetry survey indicated a maximum water depth of around 1.18, with an average depth of 0.81 m and a standard deviation of 0.25 m. The Lake Manyara has a catchment area of about 18,763 km^2 with elevations between 885 m and 3618 m a.s.l. It is a closed basin with no natural outlet [5]. The western side of the lake is flanked by a deep escarpment, while in the east an undulating plain with isolated volcanic cones gives way to a peneplain. Several springs and streams, both perennial and seasonal, drain into the Lake Manyara [5].

Figure 2. Lake Manyara seasonal rainfall pattern 1 January 2001, and 31 December 2009; created based on 11-day groups, starting in January. The upper-left frame is the normalized sum of daily precipitation rates for each case and annum pair, which sum row-wise to the upper-right frame to present annual precipitation totals; the lower-left frame is sorted vertically to represent the sample quantiles, and is contoured; the lower-right frame is the row-wise sum of sample quantiles; the vertical (red) line indicates the median of the annual sums, and the horizontal line represents the seasonal 'normal' that has the same annual amount.

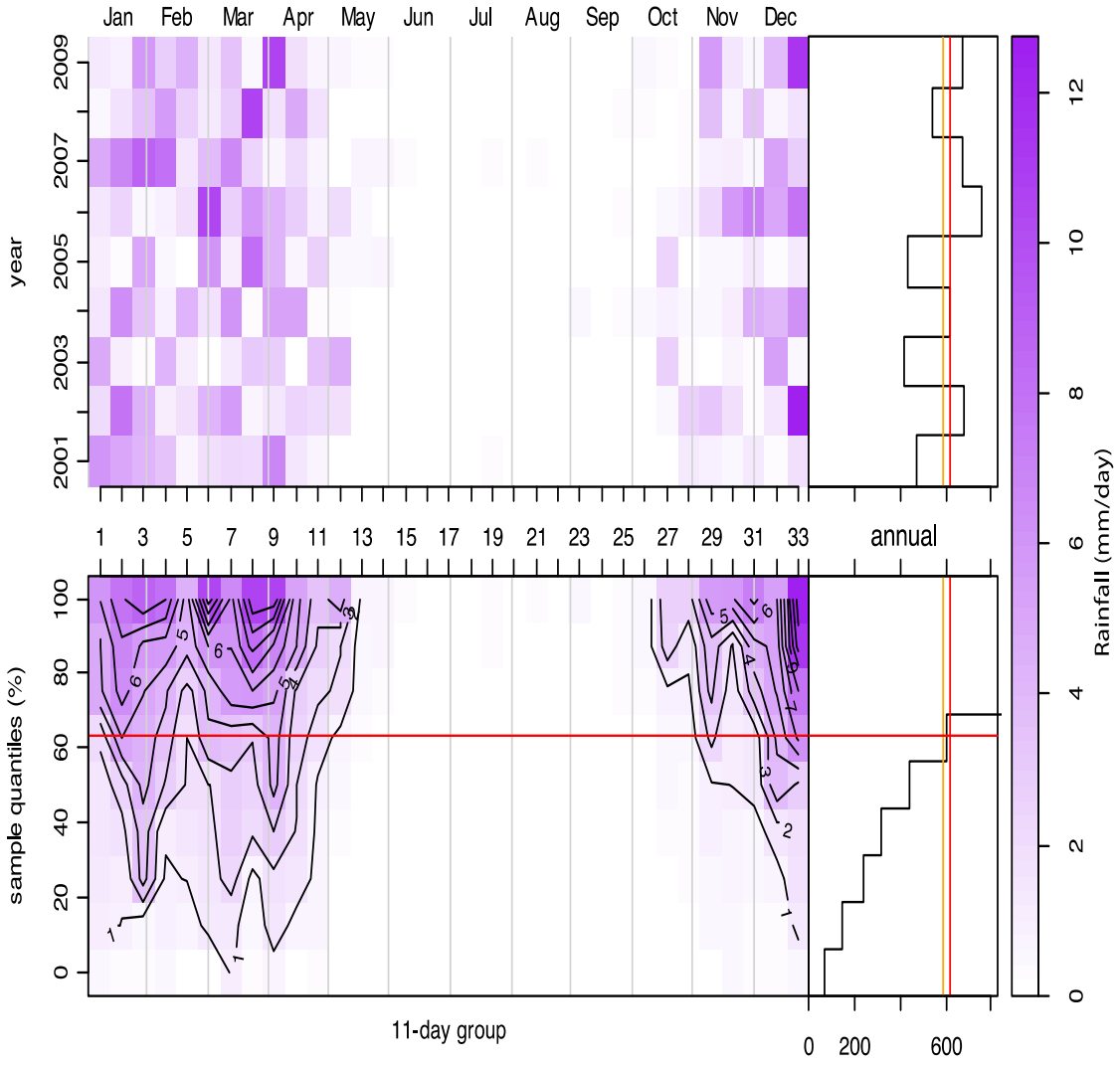

2.2. Climate

The climate of East Africa is principally influenced by the seasonal shift of the Intertropical Convergence Zone (ITCZ) [11,22] and Indian Ocean Dipole (IOD). The IOD is an ocean-atmosphere

interaction, over the Indian Ocean, creating alternating positive and negative Sea Surface Temperature (SST) anomalies. During positive phase there is flooding in East Africa. The Indian summer monsoon is more intense than normal and there is drought in Indonesia and in several regions of Australia [23,24].

The Lake Manyara basin lies within a semi-arid to semi-humid tropical climate zone characterized by high evaporation rate and low rainfall. In semi-arid regions, rainfall events are of short duration and high intensity and often characterized by a large degree of spatial heterogeneity [3,25,26]. Lake Manyara has highly seasonal and annually variable rainfalls of approximately 600 mm/yr (Figure 2).

In general, the rain season lasts from November to May with a short and a long rainy season. The short rains (Vuli) occur between November and January. These rains can be interrupted by a short dry season in January and February. The long rains (Masika) occur between February and May. The dry season from June to October is consistent through the years and lengthens when the short rains fail [27,28]. Daily average air temperatures at the lake range from 14 ℃ to 30 ℃, with peaks from December to February (Figure 3). Figure 3 shows the relations of both mean temperature variability and diurnal variability throughout the two distinct seasons over the study period (2001–2009).

Figure 3. Lake Manyara temperature normal 2001–2009. Boxplots are from daily mean values and red vertical lines represent diurnal variability as derived from median, daily maximum and minimum temperatures.

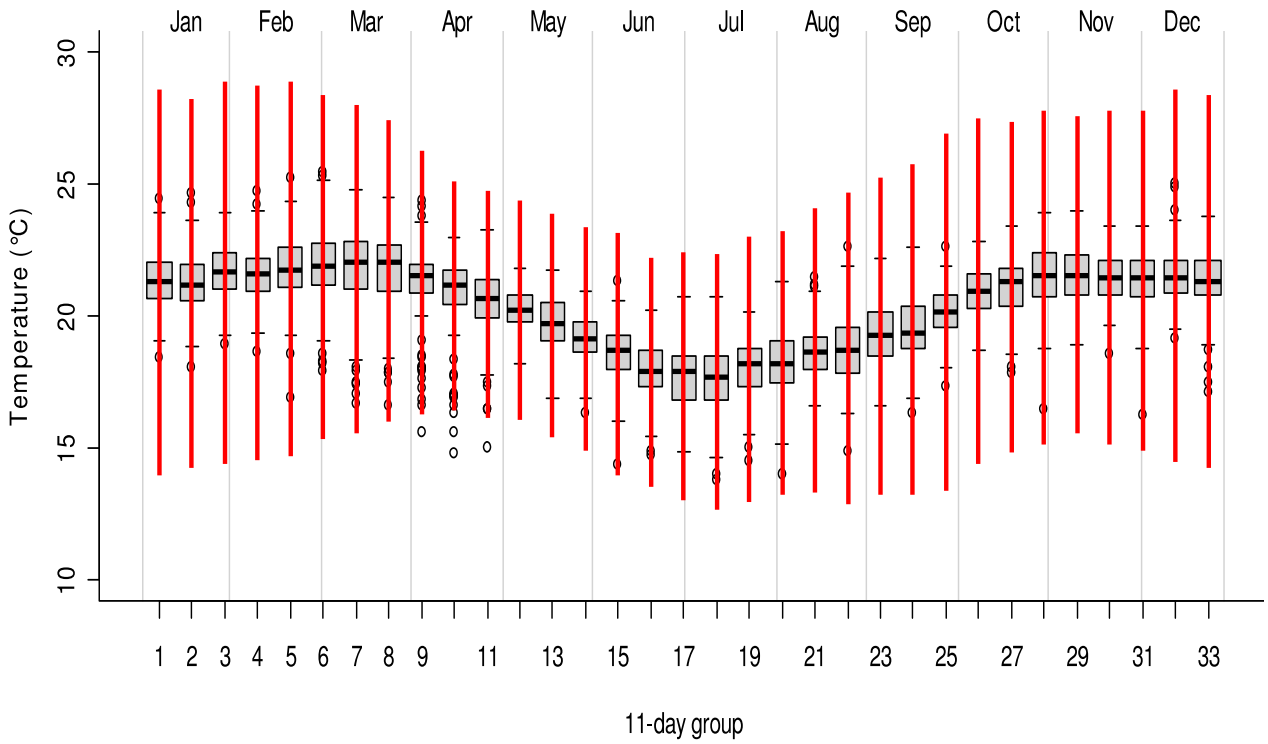

3. Data and Parameters

3.1. Data Sets

In situ data availability for hydrological modeling is a great challenge at Lake Manyara and its surroundings. Limited information concerning the Lake and its catchment in general is available as the lake is un-gauged and the basin poorly gauged. The hydrological observation network is very sparse

and the number of gauging stations has been decreasing since the 1990s. In the same time more satellite-based techniques provide us with potential continuous hydro-meteorological data, which can be used in hydrological models. In this study, we apply different types of data based on ground and remote sensing measurements as inputs to a hydrological model. We use land cover types extracted from Moderate Imaging Spectroradiometer (MODIS) derived land cover product (MOD12Q1). This product is based on the International Geosphere-Biosphere Programme (IGBP) classification scheme [29] and has a spatial resolution of 500m. For topographical information we used the Shuttle Radar Topographic Mission (SRTM) digital elevation model (DEM) with 90 m resolution [30,31].

Figure 4. (**a**) Comparison of GPCP precipitation and rain gauge data; (**b**) TRMM 3B43 V7 accumulated precipitation and rain gauge data; (**c**) GPCP as related to TRMM 3B43 V7 precipitation product.

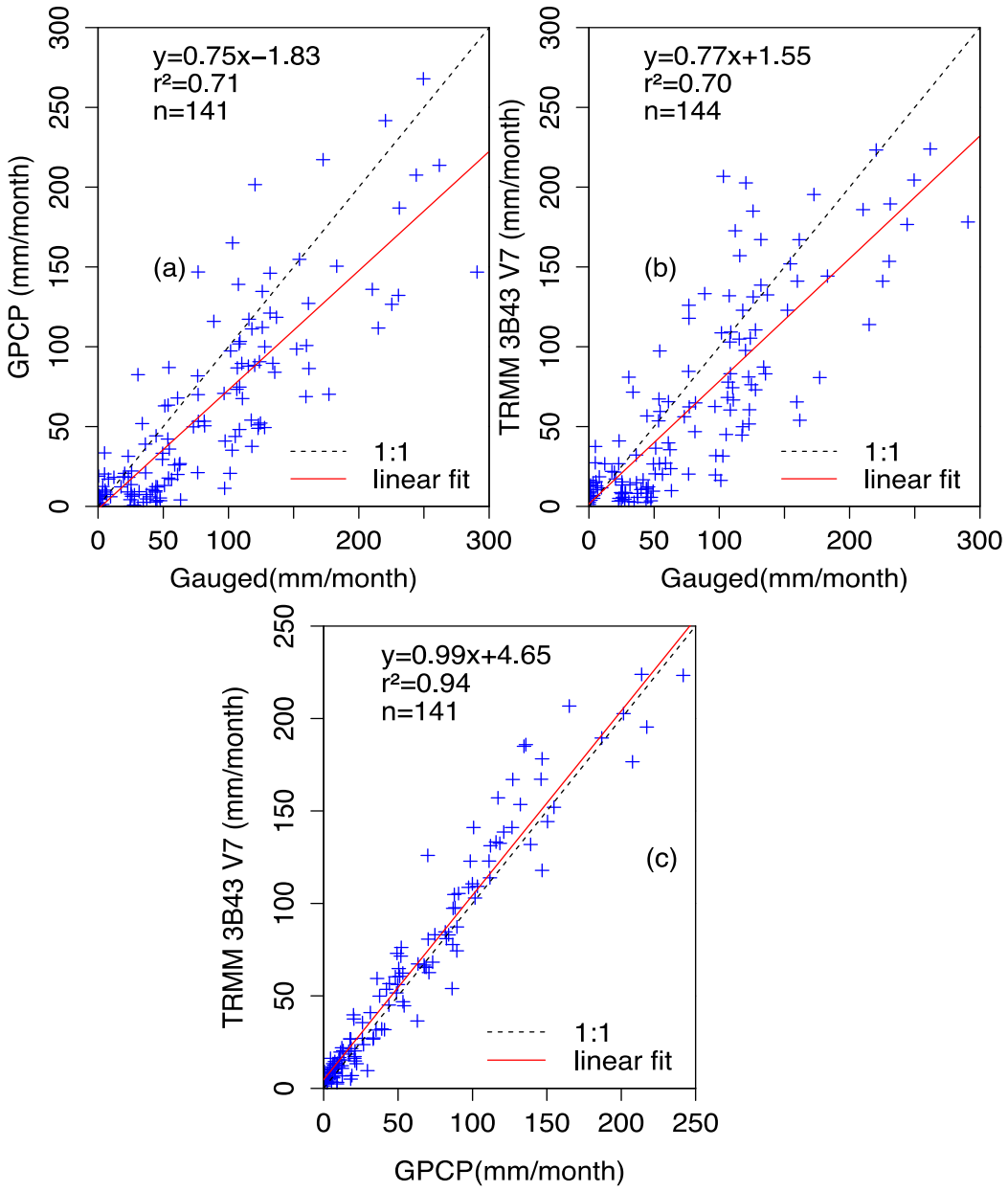

3.1.1. Remote Sensing Observation

Rainfall

Rainfall is the most essential component for water balance estimations. It is a key forcing variable in hydrological models. Hence, spatially and temporally correct rainfall measurement is critical for hydrologic modeling and thus the management of water resources, especially in semi-arid regions [11,32,33]. We tested *in situ*, Tropical Rainfall Measuring Mission (TRMM) and Global Precipitation climatology (GPCP) rainfall products. TRMM combined precipitation product (3B43-V7) with a spatial resolution of $0.25° \times 0.25°$ is used to characterize the most important input parameter for the Manyara basin water balance [34]. We acquired the TRMM 3B43 V7 monthly rainfall estimate from January 2001 to December 2009. TRMM data are suitably accurate even for mountainous areas [35]. GPCP rainfall product combines microwave and infrared satellite observations as well as rain gauge data. GPCP provides a record of almost 30 years of global monthly precipitation and daily rainfall starting in 1979 [36–38]. *In situ* and GPCP precipitation datasets are used for validation purpose. We checked the suitability of the TRMM data in the Manyara basin with a comparison of TRMM 3B43 V7 accumulated precipitation product with *in situ* and GPCP data (Figure 4). GPCP precipitation product for the field area gives a coefficient of determination, r^2 of 0.71 (Figure 4(a)). TRMM displayed the coefficient of determination of 0.7 (Figure 4(b)). GPCP and TRMM 3B43 V7 rainfall dataset are related with the coefficient of determination, of 0.93 (Figure 4(c)). This signifies that both TRMM and GPCP, alone or jointly, have the potential to supersede *in situ* data for hydrological studies in the region. Both TRMM 3B43 V7 and GPCP rainfall products tend to underestimate precipitation in the catchment.

Temperature

There are no remote sensing products for air temperatures available so far. We used MODIS/Terra (Earth Observing System (EOS) AM-1 platform) day and night time MOD11C1 V5 land surface temperature (LST) product at a spatial resolution of $0.05° \times 0.05°$ [39] to estimate water balance in Manyara catchment. Ruhoff *et al*. [40] used MODIS LST to estimate energy balance in Brazilian tropical savannah. Wan *et al*. [41] validated the accuracy of daily MODIS LST products in more than 20 clear-sky cases with *in situ* measurement. They found that MODIS LST accuracy is better than 1 K in the range from $-10°$ to 50 ℃. Furthermore, Wan *et al*. [39] compared MOD11C1 V5 LSTs in 47 clear-sky cases with *in situ* measurement and reveal that the accuracy is better than 1 K in the range from $-10°$ to 58 ℃ in about 39 cases.

Since we use both *in situ* air temperature and MODIS LST; we compare monthly mean MOD11C1 LST product over the study area with monthly mean *in situ* air temperature dataset covering the 2003–2006 period (Figure 5).

We compare the average of MOD11C1 V5 LSTs with measurements from three meteorological stations located in East Africa, namely Arusha, Kilimanjaro International Airport (KIA) and Jomo Kenyatta International Airport (JKIA). We find out that monthly daytime LST closely fits with the *in situ* maximum air temperature data. The Pearson's correlation coefficient (r) values were 0.82, 0.86,

and 0.73; whereas coefficients of determination (r^2) were 0.68, 0.74 and 0.54 for Arusha, KIA and JKIA meteorological stations, respectively.

Figure 5. Comparison of MODIS day and night LST and minimum and maximum *in situ* air temperature over three stations in East Africa for all temperature values, and values below 30 ℃, RSE stands for regression standard error.

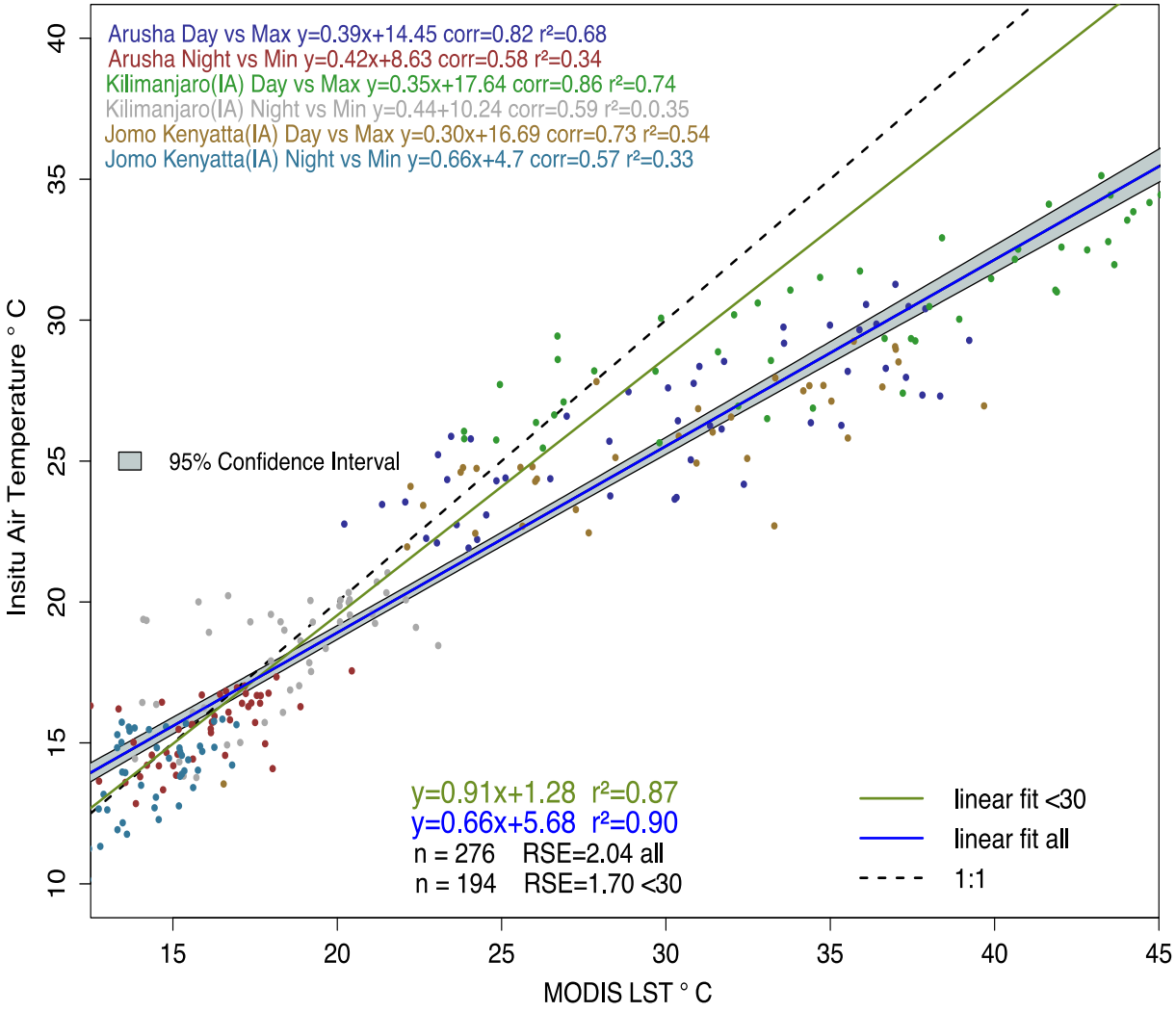

On the other hand, the monthly night time LST product showed lower r coefficients (up 0.59; and their respective r^2 up to 0.34, Figure 5). Air temperature varies between 14 ℃ and 30 ℃, and we check the overall correlation between the two time series datasets for all three stations. We apply a linear regression over (a) all values in the time series and (b) values that are less or equal to 30 ℃. The complete series give us a coefficient of determination r^2 of 0.9 (Figure 5) and temperature less or equal to 30 ℃ gives us 0.87 (Figure 5). The regression standard error (RSE) is 2.04 and 1.7 respectively. We observe that MOD11C1 V5 product best fit the *in situ* air temperature over northern Tanzania and southern Kenya. Based on our comparison (Figure 5) we argue that LST can be used to approximate air temperature in East Africa.

GRACE Equivalent Water Thickness

The GRACE satellite project is administered by the US National Aeronautics and Space Administration (NASA) and the German Aerospace Centre (DLR). The mission was launched in March 2002 in order to provide spatio-temporal variations of the Earth's gravity field over various time scales (month to decadal) [42]. Changes in gravity field are mainly due to redistribution of mass within the Earth and on or above its surface [43]. Monthly changes in earth's gravity fields can be used to derive global estimates of total water storage (TWS) with a spatial resolution of 100 km and above, with higher accuracies over larger spatial scales [14,44]. In this study we used the most recent land mass grid of GRACE data release (RL04) from the University of Texas Centre for Space Research (CSR) [45]. TWS data is available as monthly $1° \times 1°$ grids TWS over land, expressed in units of equivalent water thickness. To validate our model results and test the applicability of the dataset we used a dataset of 89 months covering the period from August 2002 to December 2009 including one missing month (June 2003).

Altimetric Lake Height

The principal focus of a satellite altimeter is to map oceanic sea surface heights. However, over recent decades they have also been used to detect water level changes in lakes and inland seas [24,46]. We investigate lake levels for two lakes in the vicinity of Lake Manyara, Lake Victoria and Lake Rukwa. The data is provided by the *Laboratoire d'Etudes en Geodesie et Oceanographie Spatiales* (LEGOS) from the *Oceanographie, et Hydrologie Spatiales* (GOHS). The LEGOS/GOHS time series are based on data from a combination of satellites: Topex/Poseidon, ERS-2, GFO, Jason-1, and ENVISAT. We use altimetric height levels from the period of January 2002 to December 2009.

3.1.2. *In situ* Datasets

We use different types of ground measurement and geographical information system (GIS) data to extract model parameters as input and drivers for model simulation and for validation of remote sensing observations and results. The hydro-meteorological dataset includes monthly records of rainfall, temperature (maximum, minimum and mean), evaporation, relative humidity, sunshine duration, wind speed and discharge data. There are about four rain gauges within the catchment, two discharge stations and one meteorological station around Lake Manyara that provide reliable data. Soils information is taken from the harmonized world soil database (HWSD) [47]. This geological information was digitized from a 1:1,000,000 geological map of Tanzania of 2004.

3.2. Model Input Parameters

We tested both *in situ* and remote sensing data in the J2000g hydrological model (Figure 6). The model requires two types of input values: temporally varying time series data and temporally static GIS information. The time series data includes relative humidity, sunshine duration, maximum, mean and minimum temperature, wind speed, precipitation and observed runoff. The second input is what we refer as spatially distributed parameters about (1) land use/land cover such as albedo, stomata conductance (Rsco), maximum plant height (H_{max}), leaf area index (LAI), maximum root depth

(RD_{max}) and minimum surface resistance for water-saturated soil (Table 1); (2) soil thickness and useable field capacity per decimeter of profile depth; (3) the maximum possible percolation rate (ground water recharge rate) per time interval in mm per time unit; (4) mean elevation, slope and aspect. Accurate parameterization of surface albedo is important in modeling energy balances of a given land cover [48]. We adopted albedo values from Strugnell *et al*., [49]. Stomata conductance is a fundamental factor in many ecological models and plays a significant role in the plant-atmosphere water exchange [50]. We used stomata conductance values based on Lambin [51] and Yucel [52]. The maximum plant height (Hmax) is used to determine the aerodynamic resistance of the vegetation, which in turn is used to calculate potential evapotranspiration. We adopted typical values for the maximum plant height of different species from Breuer *et al*., [53]. LAI is used to calculate the stomata resistance of the vegetation cover. The effective rooting depth of plants determines the maximum depth of water and nutrient uptake from the soil profile. We acquired LAI values from Ge *et al*., [54] and Breuer *et al*., [53]. Maximum root depth RD_{max} depends largely on soil texture, compaction, underlying bedrock, clefts, and further physical and chemical properties of the soil [53]. We employed rooting depth values from Zeng [55].

Figure 6. J2000g model input parameters for both simulation and validation.

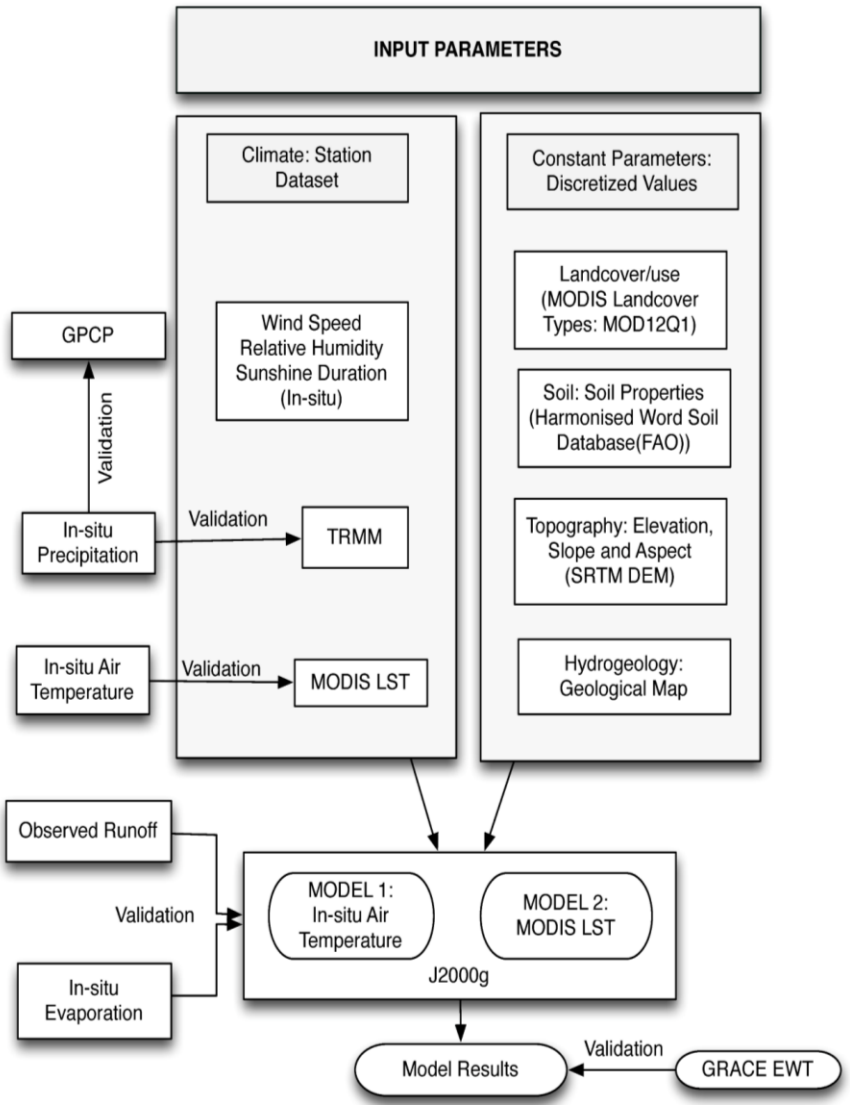

Table 1. Adopted Albedo, LAI, R_{sco}, H_{max} and RD_{max} values for each International Geosphere-Biosphere Programme (IGBP) land cover type. NA = Not Applicable. (Source: [49,51–55]).

Land Cover Type	Albedo (%)	R_{SC0}(s/m)	LAI	H_{max} (m)	R_{Dmax} (dm)
Water	0.08	NA	NA	NA	NA
Evergreen broadleaf forest	0.14	100	6	3	22
Deciduous broadleaf forest	0.16	100	6	3	20
Mixed forests	0.16	125	2	10	22
Closed shrub land	0.22	100	5	3	22
Open shrub lands	0.22	100	1	3	22
Woody savannahs	0.15	100	6	2	17
Savannahs	0.18	100	4	2	22
Grasslands	0.22	50	2	1	15
Permanent wetlands	0.16	150	1	0	1
Urban and built-up	0.18	200	3	2	15
Cropland-natural vegetation	0.17	50	4	1	15
Barren or sparsely vegetated	0.27	1	1	0	22

4. Methodology

4.1. Water Balance

In this study the spatially distributed conceptual water balance model J2000g has been selected to simulate and quantify the main water budget parameters for Lake Manyara and its surroundings [9]. The model is implemented in the Jena Adaptable Modelling System (JAMS) framework [56]. A water balance model is a mathematical expression that describes the flow of water in and out of a hydrological system such as a drainage basin or lake. It is based on the mass and energy conservation principle within an identified domain and specified time period. Dingman [57] explained that water balance is the change in water quantity for a specific control volume over time. The catchment water balance [58,59] is expressed as:

$$\frac{ds}{dt} = P - ET - Q \quad (1)$$

where ds/dt the change in storage for a certain interval of time, P is precipitation, Q is runoff and ET is evapotranspiration.

However, for the lake catchment water balance, estimations of both aquatic and terrestrial processes must be considered. Given the values for the amount of precipitation, lake evaporation (E) and evapotranspiration while assuming a homogeneous substrate throughout the lake's catchment, the water balance of the entire catchment can be expressed as a sum of the water balance from the terrestrial part of the lake catchment (LT) and that of the lake surface area (LA) [60]. In groundwater systems, outputs from a catchment occur through underground water flow from the lake (U) or base flow (subsurface runoff) and overland flow (Q) or surface runoff and balance the inputs to the catchment as [60]:

$$U + Q = LT(P - ET) + LA(P - E) \quad (2)$$

The input and output components of the water balance of a lake depend not only on the physical dimension of the water body, but also on the climatic, hydrological and geological factors affecting the water body and its surrounding areas [61]. For lakes surrounded by a small catchment basin area, the water balance is more strongly driven by evaporation than by evapotranspiration. On the other hand, lakes with a large catchment basin area relative to the lake surface area reflect a water balance more closely linked to the value of precipitation minus evapotranspiration such that the lake water balance is driven by a weighted combination of P-ET and P-E [60]. For Lake Manyara, by neglecting the change in storage over a long period we identify the principal component of the water balance to be precipitation on the lake, inflow (Q_{in}) to the lake and lake evaporation. Thus, the lake water balance (WB) can be expressed as:

$$WB = P - E + Q_{in} \quad (3)$$

Q_{in} can be further decomposed in to:
$Q_{in} = Q_{direct} + Q_{baseflow}$

where Q_{direct} and $Q_{baseflow}$ represent surface and subsurface runoff respectively. Each term describes the spatial average taken over the entire lake area.

4.2. Evapotranspiration

Evapotranspiration (ET) is the most important of water balance computations in a semi-arid climate [62]. It is a crucial factor between land, water surface and the atmosphere. In semi-arid regions the evaporation from the bare soil assumes a greater importance relative to transpiration from plants. This is due to the larger area of bare soil and the frequency of small rainfall events [3,26]. A broad analysis of the ET processes and determination of spatial and temporal ET and P estimates are required to obtain reliable estimates of water balance, as the difference between P and ET defines what is left for runoff generation. We calculate both actual and potential ET using the Penman-Monteith approach [63] implemented into J2000g. The Penman approach combines the fact that evaporation is a diffusive process and that energy can be expressed in terms of mass [64]. The Penman-Monteith equation refines weather-based potential evapotranspiration (PET) estimates for vegetated land areas and is widely regarded as one of the most accurate models, in terms of estimates based on physical background. The model requires daily mean temperature, wind speed, relative humidity, and solar radiation to calculate potential ET. Actual evapotranspiration (AET) is estimated in J2000g from PET and the actual water content of the soil storage.

To compute evaporation from the lake we use the approach of Penman [65]. Evaporation from lakes is a key constituent of the water balance; hence its accurate determination is essential for a reasonable estimate of the water balance. The Penman method has been found suitable for evaporation estimation under any climatic conditions and for a time scale of up to one month [66].

4.3. Model Setup, Calibration and Validation

4.3.1. Model Setup and Parameterization

The performance of a model in terms of prediction depends on the setup and parameterization. The J2000g water balance model setup involves catchment and parameter discretization into a spatially distributed format, selection of initial calibration parameter values and time setup. The model is simplified to temporally aggregate and spatially distribute the hydrological parameters to be calculated. The representation and calculation of the hydrological processes in the model is carried out in one-dimension for any number of points in space. The catchment basin was then discretized into grid cells, each with a spatial resolution of 1 × 1 km². All physical parameter layers were translated to exactly the same extent in terms of projection and were re-sampled to pixels of 1 by 1 km so as to overlay the parameters belonging to the same grid entity correctly. This implies that inside one modeling grid there is one value parameter for each land cover type, soil, permeability, slope, aspect, and elevation.

We performed the temporal discretization of the modeling steps on a monthly basis. We computed the following processes for each time step during modeling: the regionalization of climate data to the modeling units, calculation of global and net radiation as inputs for the evaporation calculation, calculation of land cover specific potential evaporation according to the Penman-Monteith equation, soil water balance, groundwater recharge and discharge delay. More details are given in [9].

4.3.2. Model Calibration and Validation

The reliability of model predictions depends on how well the model structure is defined and how well the model is parameterized [67]. Estimation of model parameters is normally sensitive and challenging due to uncertainties associated with the determination of parameter values that cannot be obtained straight from the field. Hydrological models are calibrated by tuning sensitive model parameters in order to obtain a good match between simulated and observed discharge time series. This classical calibration approach was not suitable for the Lake Manyara catchment because only a very short time series of two month with daily data from the subcatchment of the Simba River that flows into the lake coming from north (Figure 1) was available. Because of the limited amount of discharge data we setup a daily model first to obtain a set of reasonable parameter values and to find out if the model can be used in the Lake Manyara region driven by the remote sensing input data. Furthermore, we used the model to get information about parameter sensitivity in terms of water balance and hydrograph dynamics. J2000g has four calibration parameters, which influences runoff generation and which react with different sensitivity on the hydrological balance. Parameter field capacity adaptation (FCA) controls the dimension of the soil water storage. An increase of the parameter results in a decrease of runoff generation and an increase in evapotranspiration. Parameter ET reduction (ETR) controls the calculation of actual evapotranspiration depending on potential evapotranspiration and soil water content. The larger the parameter is the more soil water can be evapotranspirated. Parameter lateral vertical distance (LVD) is responsible for the partitioning of the total runoff generation into direct runoff and baseflow. The larger LVD is the more direct runoff is generated. In terms of the total water balance, LVD is not sensitive. Parameter maximum percolation

adaptation (MPA) limits the groundwater recharge to a maximum value per time step that cannot be exceeded. This parameter is also not sensitive on the water balance. Because no sufficient information was available about groundwater recharge, we put the parameter MPA to a very high value, which practically eliminates its impact. Two additional recession parameters control the dynamics of the direct runoff (DK) and the baseflow (BK). Both parameters are not sensitive for the water balance but can act very sensitive on the shape and timing of the simulated hydrograph.

The six parameters of the daily model were calibrated manually to provide a reasonable fit between observed and simulated runoff (Table 2).

Table 2. Model parameters from the calibrated daily model along with parameter boundaries for sensitivity analysis.

Parameter	Cal. Value	Upper Boundary	Lower Boundary
FCA	2.65	2.385	2.915
LVD	2.84	2.556	3.124
ETR	0.8	0.72	0.88
MPA	100	90	110
DK	4	3.6	4.4
BK	21	18.9	23.1

The result of the manually calibrated model for the Simba River is shown in Figure 7(a,b). The plot shows that the model was able to reproduce the overall dynamics and magnitude of the observed runoff. In the first half, the runoff was underpredicted by the model whereas in the second half the model was slightly over predicting. Both problems are related to the short period, which was not sufficient to provide a proper warm-up period for the model. To provide an objective classification of the model quality we calculated a number of objective functions. Here we obtained a value of 0.35 for the Nash-Sutcliffe efficiency [68], 0.54 for r^2, a relative volume error (PBIAS) of −25 %.

To evaluate the sensitivity of the model parameters and to reflect the uncertainty from model parameterization we applied a uniform-random-sampling of all parameters with the parameter boundaries shown in Table 2 and a sampling size of 200. For each parameter set the efficiency parameters were calculated. The analysis showed that DK had the highest sensitivity in terms of NS whereas in terms of pbias FCA reacts most sensitive. All other parameters did show only low sensitivities compared to DK and FCA. The envelope of the 200 random model realizations is shown in Figure 7(a). The plot shows that the uncertainty from model parameterization is largest during peak flow and the falling limb of the hydrograph and that the observed runoff is often outside the uncertainty band. Taking the short time series and the unclear quality of the observed runoff data into account we decided that the model is good enough to be used for the entire catchment.

From the daily model a monthly model was derived by transferring the model parameters. The monthly model does not need a recession parameter for the direct runoff as it can be expected that the travel time of this component is below the modeling time step. The parameters controlling the runoff generation were left at the same values as in the daily model because they are independent from the modeling time step. Only the recession parameter for the baseflow component had to be adapted to reflect the changing temporal resolution.

Figure 7. (**a**) Observed and simulated runoff (Q) for Simba River along with uncertainty band, for calibration period April–June 1980 (**b**) Relationship between the average simulated runoff (AVG) and observed runoff as depicted using linear regression.

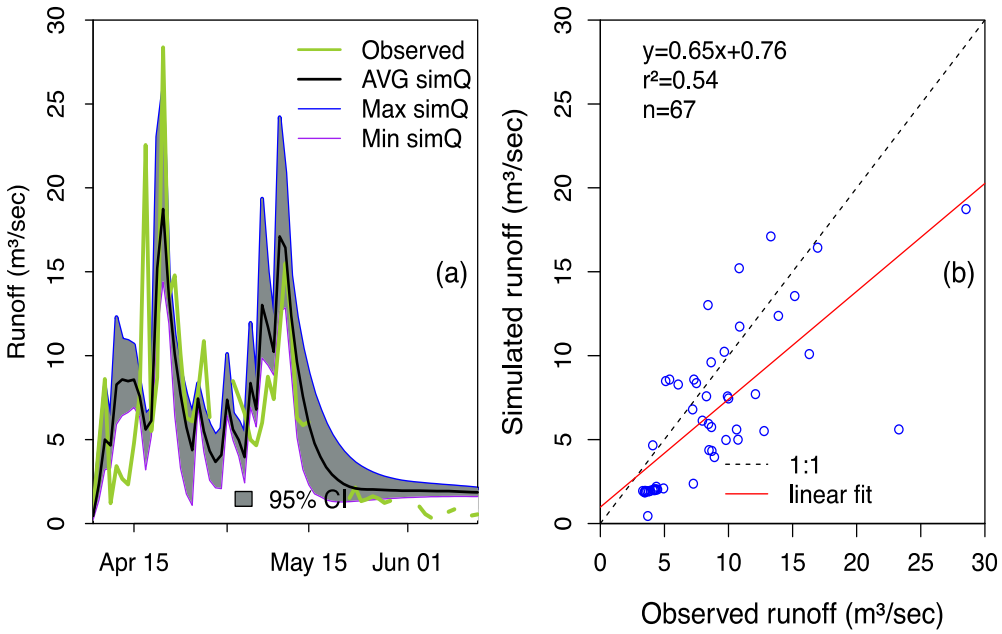

Figure 8. (**a**) Simulated and observed Evapotranspiration distribution pattern for the validation period (2002–2006); (**b**) Scatter plot displaying a relationship between simulated actual ET and observed evaporation.

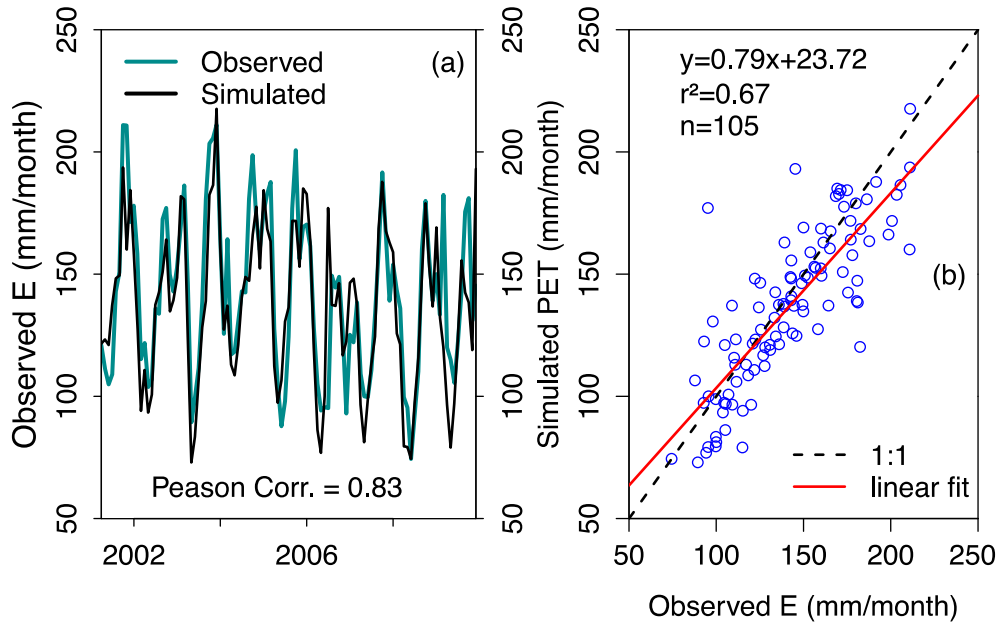

We validated the monthly model using a nine year (2001–2009) evaporation dataset from pan evapotranspiration in the north eastern part of the basin (Figure 8(a,b)). Based on the Pearson correlation, observed and simulated actual evapotranspiration are interrelated with a correlation coefficient, R = 0.83 and the r^2 = 0.67. We observed that the model slightly underestimates ET during periods with a low ET rate. This might be attributed to the accuracy of satellite observation data used.

5. Modeling Results and Discussion

5.1. Monthly Basin Water Budget Components

We simulated the spatial-temporal variation of the water balance components on modeling grid cell resolution. We forced two separate models, with *in situ* air temperature and MODIS LST. The results from the two models are comparable. The mean monthly air temperature ranges between 14.4 ℃ and 25.8 ℃. Relative humidity was computed as 82% in a long term mean with values between 68% and 92%. For the study period, a mean air temperature of 20 ℃ was simulated for the Manyara basin. Monthly variations in the time series results of the hydrologic water balance variables are presented in Figure 9. We observe a huge increase in runoff in January 2007. We suggest that the increase might be attributed to the strong influence of Pacific and Indian Ocean sea-surface temperatures (SST) such as El Niño-Southern Oscillation (ENSO) and Indian Ocean Dipole (IOD) [12,68,69].

Figure 9. Monthly variation of the components of water balance in Lake Manyara basin during the study period. RSW = Relative soil water, Max and Min stands for maximum and minimum predicted values and CI = confidence interval.

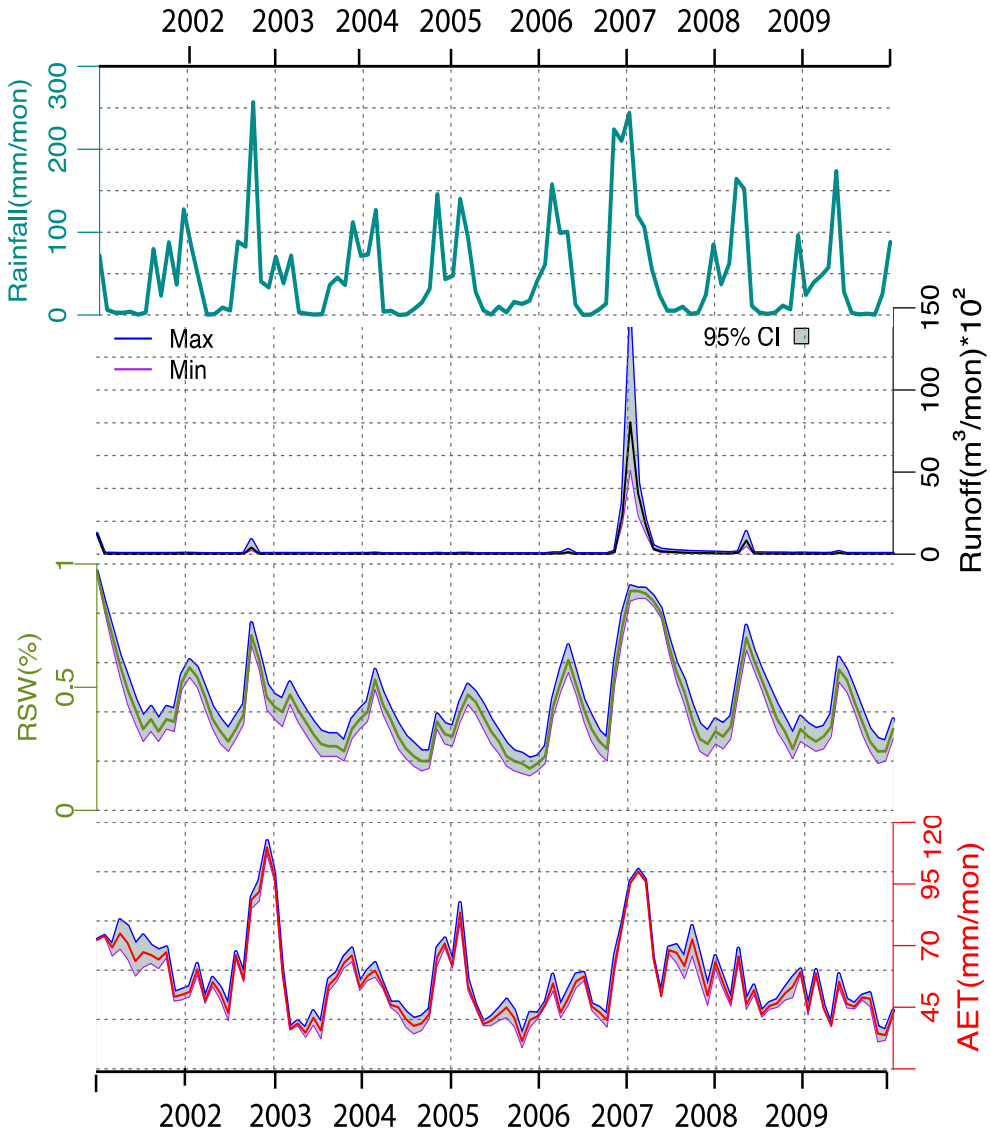

Figure 10 presents the mean monthly water budget elements in Lake Manyara basin over the study period. We observe that monthly mean runoff and ground water recharge display the same distribution pattern. The actual evapotranspiration is high in months with large amount of rainfall (Figure 10).

Figure 10. Mean monthly annual water balance parameter variation for Lake Manyara catchment (2001–2009).

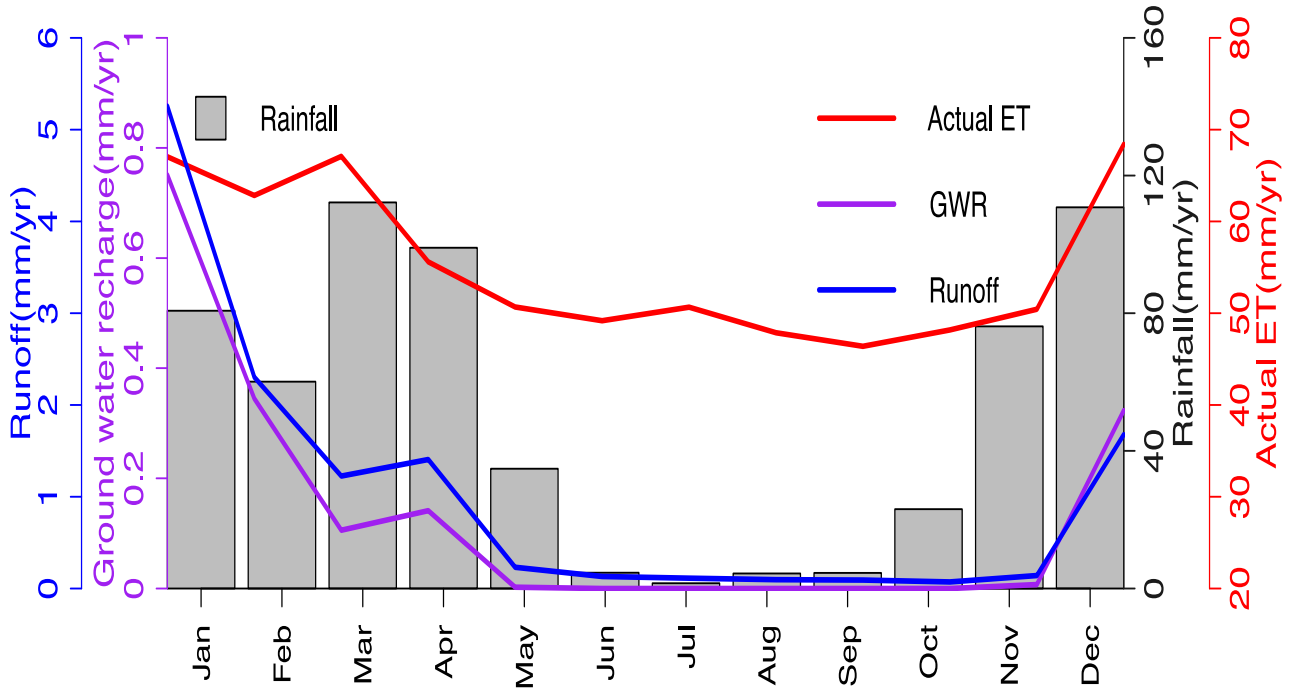

Precipitation

In the Manyara basin, as in other semi-arid regions, precipitation events are of short duration and high intensity and normally characterized by high spatial and temporal variability. The mean monthly rainfall is computed to be 51 mm/month over the study period. Most rainfall events occur during the wet season. Trend analysis of rainfall results indicates that much rainfall occurred in November and December 2002 and the November 2006 to May 2007 rainy season (Figure 9). Previous studies in the east African region have related the variation of precipitation to ENSO and IOD anomalies [12,68,69].

Evapotranspiration (ET)

Around 90% or more of annual rainfall in semi-arid regions can be lost through evapotranspiration [62]. The mean monthly potential evapotranspiration (PET) is computed to be 93 mm/month. In semi-arid regions actual evapotranspiration (AET) is a key component in the hydrological cycle and may account for more than 90% of precipitation [26]. We estimate a mean monthly AET of 55 mm. Even if PET is much higher in the dry season AET is almost identical for both the dry and wet season.

Runoff

J2000g estimates runoff as the reminder of precipitation, AET and water storage in the soil or groundwater compartment. The model separates total runoff into two components direct runoff (DQ)

and base flow (BQ) A monthly mean runoff of 1.06 mm was calculated for the Manyara catchment. In general, the simulated monthly runoff shows only very small events despite one big peak in January 2007 (Figure 9), which might be related to the influence of ENSO and IOD in the region [12,68,69].

We used an annual hysteresis loop based on concentration-discharge hysteresis analysis to check the rain-runoff relationship in the catchment and to perform a linear fit [70–72]. We observed a yearly anticlockwise hysteresis loop (Figure 11), which indicates that the discharge values respond to precipitation events occurring across the catchment.

Figure 11. Annual precipitation-discharge hysteresis. Monthly precipitation-simulated runoff. Numbered centers represent monthly mean values for individual months over the study period. Bars represent 5% and 95% quantiles. The dashed line refers to the direct relationship of precipitation and resulting discharge.

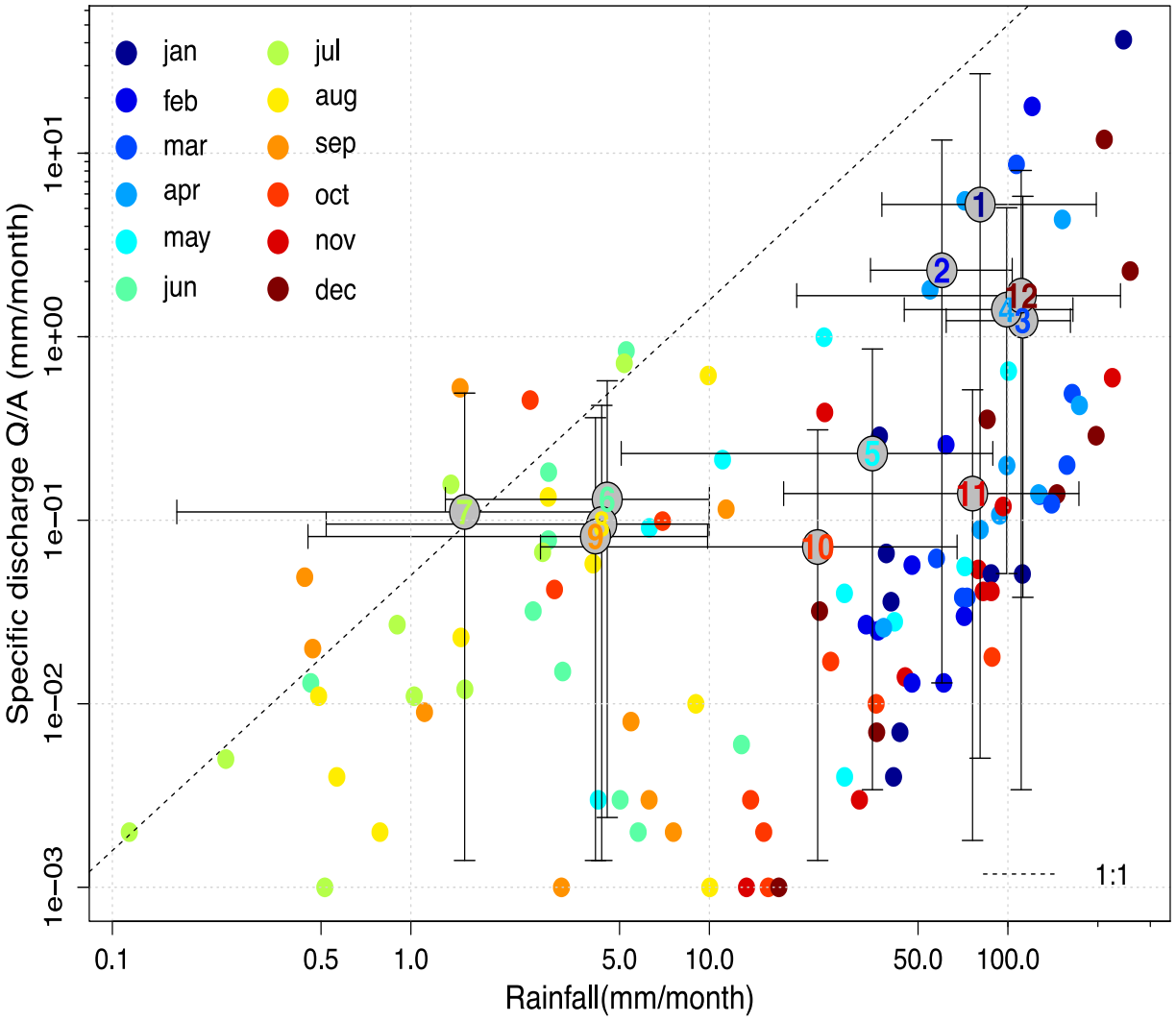

This time lag between precipitation and discharge indicates a temporal storage of water in soil or underlying rock formations. Further studies are required to specify the transient storage. The annual cycle shows that runoff values for the rainy season (November–May) are relatively high compared to the dry season (June–October), with the lowest mean monthly discharge values detected in October. The positioning of precipitation and specific discharge along the line of fit indicates a direct

relationship of rainfall and discharge. A shift of any of the precipitation-discharge pairs to an increase of precipitation indicates storage or retention while a shift toward discharge increase indicates the release of water from the catchment. We identify that there is no direct dependency between precipitation and discharge. As visible in Figure 11, there is a shift towards more precipitation. This means that most of the incoming water from precipitation is either stored in the catchment or lost through evapotranspiration during both wet and dry seasons. We suspect the latter, based on the fact that evapotranspiration accounts for 98.13% of the total outflow from the catchment basin.

Ground Water Recharge and Storage

In a semi-arid environment, groundwater is the only water resource that is available throughout the year and hence its calculation is crucial for catchment water balance estimation and sustainable management. Groundwater recharge and storage are important in water budget evaluation but challenging to quantify. Recharge cannot be measured directly and is a component of the hydrological budget that is difficult to predict. This is predominantly true for semi-arid regions where recharge may be as low as 1% of the precipitation [3,73]. In semi-arid areas ET captures most of the water entering the soil, and recharge occurs only during extreme rainfall events [26]. We estimate a mean monthly mean ground water recharge of 0.14 mm/month and ground water storage of 0.86 mm/month. Groundwater recharge displays a more or less similar trend as ground water storage. We observe in Figure 10, groundwater recharge typically increases as runoff increases. Both temperature and rainfall have an impact on groundwater recharge. Based on Figure 12, it appears that the temporal variation of soil moisture expresses as relative soil water, ground water recharge and storage is caused by climate variability; whereas their spatial variation depends on the soil, land cover and topography.

Figure 12. Mean monthly yearly water balance parameter variation for Lake Manyara (2001–2009).

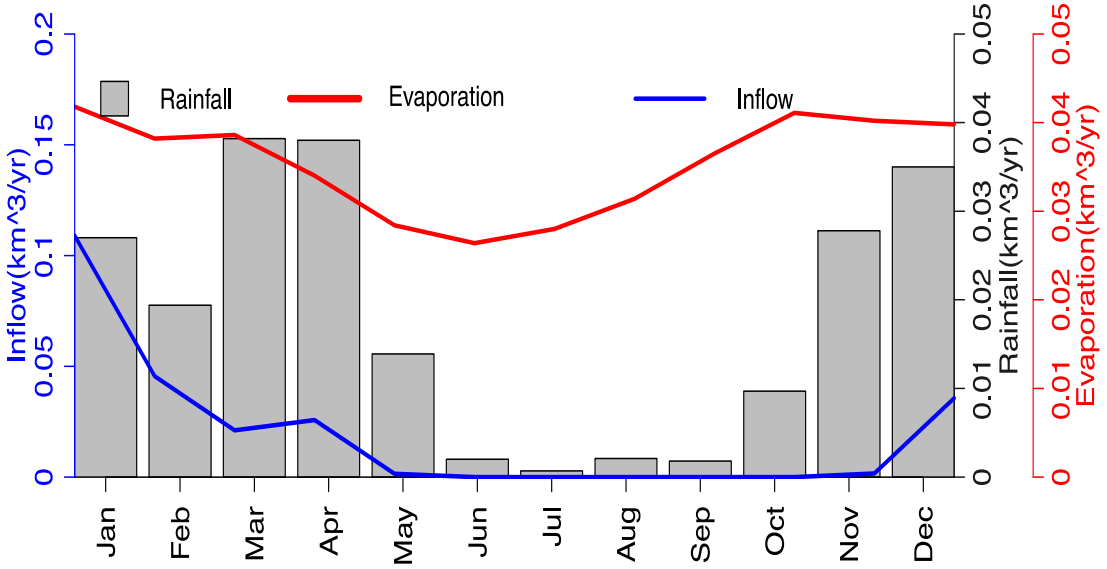

5.2. Annual Water Balance Components

We estimate the mean annual water balance components for the lake and its catchment (Table 3). The minimum annual air temperature over the study period varies between 14.03 ℃ and 14.94 ℃. The

maximum annual air temperature ranges from 25.22 ℃ to 26.29 ℃. The relative humidity varied between 80.12% and 84.03%. Annual precipitation ranged from 419 mm/yr in 2005 to 818 mm/yr in 2002. We approximate the mean annual rainfall of 612 mm/yr. Precipitation contributes 99.73% of the total annual inflow parameter in the catchment (Table 3). In simulations for lakes with a larger catchment size, almost half of rainfall in the catchment returns to the atmosphere through evapotranspiration [60]. About 108% of the total inflow to the catchment was lost through evapotranspiration during the study period for the Lake Manyara catchment basin (Table 3).

Table 3. Annual mean modeled water balance for the entire catchment (period 2001–2009). All units are in mm/yr. per year and for the lake water balance, elements are estimated in km^3/yr.

Component	Catchment Basin		Lake Manyara	
	Inflow	**Loss**	**Inflow**	**Loss**
Precipitation	611.587 (99.73%)	-	0.216 (47%)	-
ET/E	-	664.234 (98.13%)	-	0.424 (100%)
Runoff	-	12.731 (2.07%)	-	-
Inflow	-	-	0.240 (53%)	-
Ground water	1.675 (0.27%)	-	-	-
Total	613.261	676.964	0.456	0.424
Water balance	−63.703		0.032	

We estimate the mean annual potential evapotranspiration (PET) of the Lake Manyara catchment as 1120 mm/yr, varying between 1,004 and 1,221 mm/yr. This indicates that potential evapotranspiration is nearly twice the mean annually precipitation in the catchment. We compute the actual evapotranspiration to be 665 mm/yr, ranging between 573 and 702 mm/yr. The actual ET contributes with 98.12% to the annual water loss from the catchment (Table 3). The mean annual runoff is estimated to be 12.73 mm/yr varying between 0.261 and 74.94 mm/yr. We observe that discharge from the catchment contributed by 2.07% of the total annual water loss over the study period (Table 3).

We estimate a mean yearly ground water recharge and storage of 1.67 and 9.6 mm/yr respectively. The mean annual ground water recharge accounts for 0.27% of the total inflow to the catchment (Table 3). The annual catchment ground water storage ranges from −3 to 271 mm/yr.

We model the mean annual values of the key water balance parameter for the lake from 2001 to 2009. The results are given in Table 3. We calculated the annual mean rainfall over the lake to be 0.216 km^3/yr, evaporation was estimated as 0.424 km^3/yr and inflow to the lake was estimated as 0.24 km^3/yr. Inflow consists of a contribution from streams and underground springs. Rainfall contributes with 47% to the total inflow while evaporation from the lake was the largest component of the water balance, accounting for 100% of total water loss. Inflow to the lake contributes 53% of the total inflow parameter. For Lake Manyara only 7% of the total inflow did not evaporate during the study period. Figure 12 illustrates the mean monthly water balance components for Lake Manyara over the study period. We observe that the inflow to the lake is almost zero during the dry season (June–September). Figure 13 presents a catchment-scale lake water balance as a weighted combination of P-ET and P-E curves [60]. Cardille *et al*., [60] suggested that a lake with a large catchment area relative to the lake surface area reflect a water balance more closely related to the value of precipitation minus evapotranspiration.

Figure 13. Monthly means water balance parameter of Lake Manyara (2001–2009): Precipitation-Evapotranspiration (P-ET), Precipitation-Evaporation (P-E) and their weighted combination Lake Water balance.

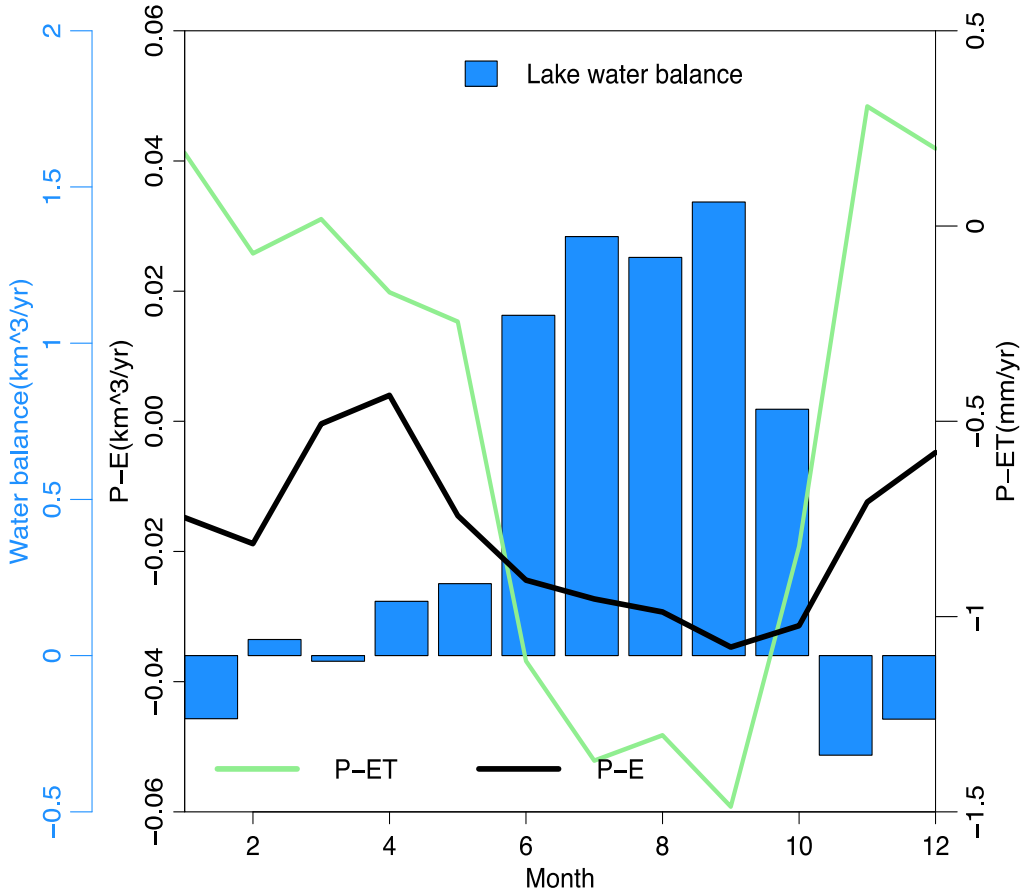

5.3. Lake Water Balance and Comparison

Due to the fact that the lake is supplied both by rainfall and stream inflow, a reduction in basin water storage causes a lake level decrease [16]. Lake morphometric influences a lake's water balance by affecting the evaporating surface area for a given lake volume and the portion of the lake bed that transmits ground water flow in and out of the lake [60]. Since Lake Manyara is un-gauged we estimated the lake capacity using the lake surface area-volume relationship at different depths by applying lake bathymetry measurements surveyed in 2010.

The Lake Manyara bathymetric map (Figure 14(a)) has been generated using an echo sounder, which measures the depth of the lake floor. The echo sounder was attached with a Global Positioning System (GPS) device to capture the horizontal position of specific points. The deepest point lies by 1.18 meters (Figure 14(a)) and the height above the mean sea level at this point is 957 m. The horizontal datum for mapping is the global datum, based on the World Geodetic Reference System 1984 (WGS84) reference ellipsoid. Figure 14 (a–c) presents a bathymetric map, lake morphology and a relation between lake surface volume and area computed at different lake levels respectively.

Figure 14. (**a**) Bathymetric map; (**b**) Lake Morphology; (**c**) Relative volume *vs*. relative area of the lake.

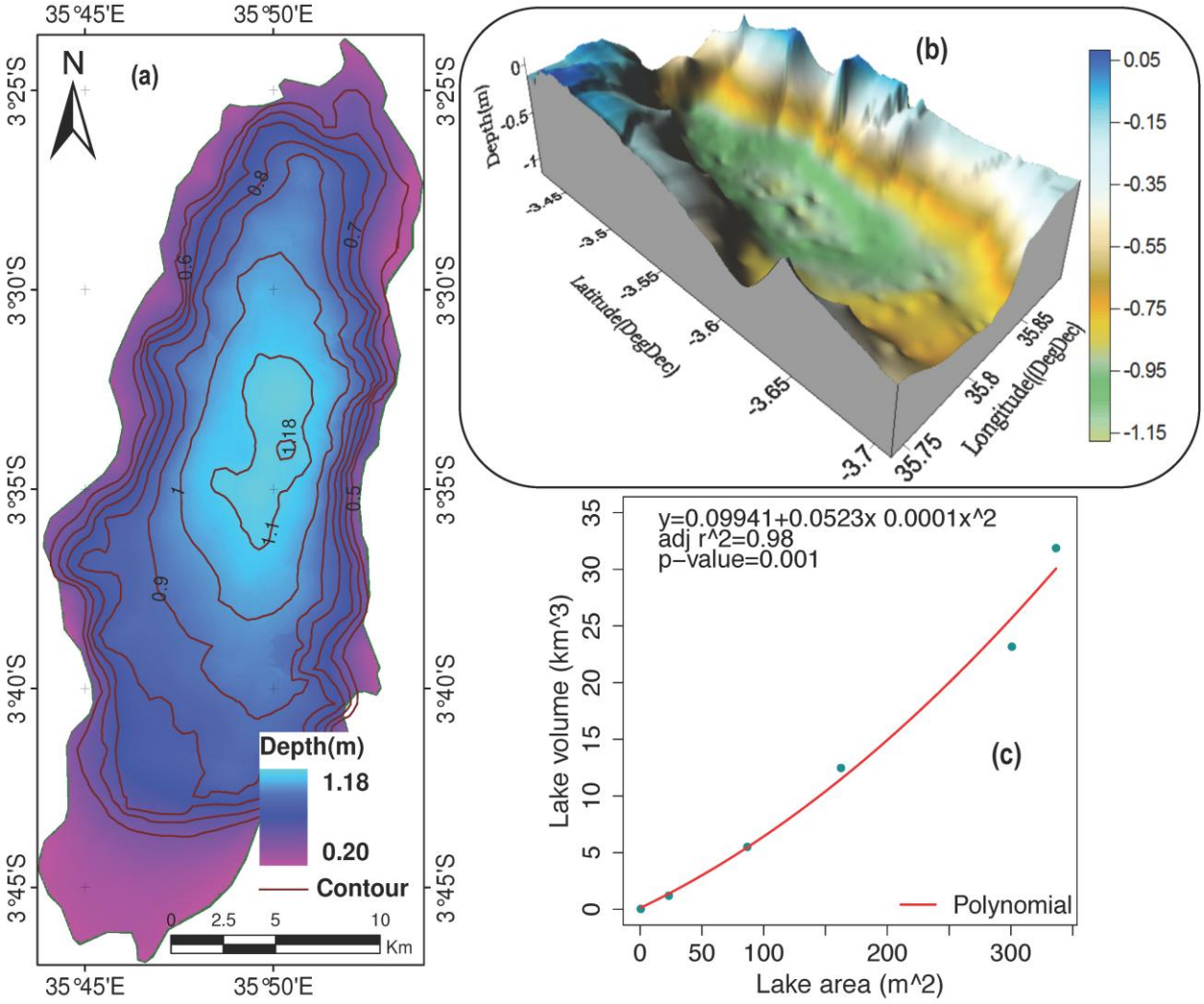

Lake Water Balance and GRACE Equivalent Water Thickness Comparison

We compare the GRACE derived total water storage (TWS) as equivalent water thickness (EWT) [17,45] with the simulated water balance from J2000g. The latest GRACE data with improved precision and resolution permits the study of smaller basins especially when the hydrological signal in the catchment is strong [12]. When the basin's hydrological signal is strong the seasonality of the water storage is large than the associated GRACE uncertainties [17,44]. We extracted a time series of GRACE equivalent water thickness for a single pixel on the Lake from the land mass grid and applied a specific scale factor [17]. We use the scale factor so as to restore a considerable amount of the energy removed during smoothing of the data using the destriping, gaussian, and degree 60 filters [17]. Figure 15(a) shows the lake water balance volume superimposed on to the GRACE equivalent water thickness along with the uncertainty bands based on the uniform random sampling of the model parameters.

Figure 15. (**a**) Lake water balance trend as compared to satellite gravimetry GRACE equivalent water thickness data. GRACE EWT data are smoothed with a six month exponential moving average window; (**b**) Lake Manyara simulated water surface height variation at 95% confidence interval (CI) as compared to neighboring lakes in East African region.

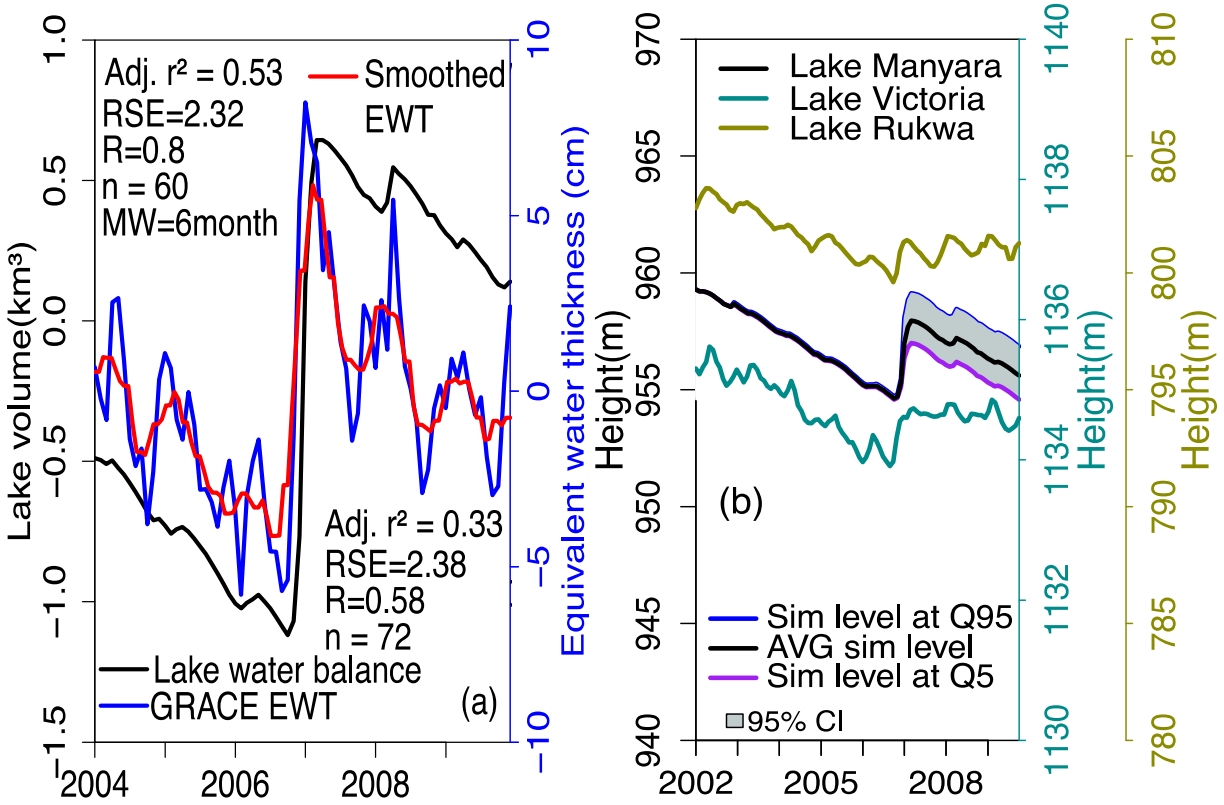

The plot shows that there is a constant decline of the lake volume in the first three years. During this time, very little inflow occurred and water was lost by evaporation. During this time, the model parameters had no impact on the simulated lake level change. In 2007, a sudden increase in the lake level occurred associated with a reasonable model uncertainty (Figure 15(b)). This uncertainty remains in the following years as kind of bias.

In Figure 15(b), the Lake water balance volume is also overlaid by the smoothed GRACE equivalent water thickness. The data are interrelated with a Pearson's correlation coefficient of 0.58 and an adjusted r^2 of 0.33 (Figure 15(a)). Due to frequent fluctuations in GRACE data we applied a 12-month exponential moving average (EMA) to smooth the dataset and elude small-scale noise. The exponentially smoothed GRACE equivalent water thickness improves the relation between the two datasets. After this step, we obtained the Pearson's correlation coefficient of 0.8 and an adjusted r^2 of 0.53 (Figure 15(a)).

We observe an abrupt change in GRACE equivalent water thickness and in the lake water balance volume between 2006 and 2007. Similarly, Becker *et al*. [12] discovered sudden changes in GRACE total water storage and water surface volume for several lakes in East Africa for the same period. The variations are directly correlated to the strong positive and negative episodes of Pacific and Indian Ocean sea-surface temperatures (SST) such as El Niño-Southern Oscillation (ENSO) and the Indian Ocean Dipole (IOD) in 2006–2007 [68,69].

We used a trend analysis to compare the simulated lake water balance with GRACE equivalent water thickness. To quantify whether trends are significant or not a signal to noise ratio (SNR) was calculated as the ratio between the estimated trend and the standard deviations of the anomalies. Signal to noise ratio values ≥1 indicate a significant trend [74,75]. Unfiltered GRACE equivalent water thickness data gave a trend that was not significant (SNR = 0.16). By contrast, smoothed GRACE equivalent water thickness exhibited a significant linear trend (SNR = 3.49). The monthly anomaly was calculated by subtraction of the 2001–2009 monthly mean from the monthly EWT data.

Using satellite altimetry, we compared Lake Manyara water level fluctuations with two lakes in the vicinity (Figure 1): Lake Victoria and Rukwa (Figure 15(b)). Satellite altimetry has been employed to monitor water levels of lakes, flood plains and wetlands over the last two decades [12–14,24,46,76–78]. As it can be observed in Figure 15(b), the simulated Lake Manyara water level varies in similar fashion to other lakes in the region.

6. Conclusions

The aim of this work was to use remote sensing datasets to investigate the water cycle of a poorly gauged lake catchment where local *in situ* measurements are limited or even unavailable. Specifically, we have quantified successfully the catchment water balance components. We examined the applicability of the J2000g hydrological model in a data poor semi-arid lake basin. We tested the utility of GRACE satellite gravimetry total water storage (TWS) data on small un-gauged lake catchment basins and minor lakes that are not included in the global satellite altimetry mission network and obtain promising result.

To achieve our objectives we employ both *in situ* and remotely sensed data in the J2000g semi-distributed hydrological model. We found that rainfall contributed up to 99.73% of the total annual inflow parameter in the catchment while ground water recharge accounts for only 0.27%. The actual ET is the most important water balance component and accounted for 98.12% of the water loss from the catchment. Discharge from the catchment contributed with 2.07% to the total annual water balance. Our result indicates that a reasonable simulation of the surface water cycle can be attained in un-gauged area using remote sensing datasets. We show that *in situ* air temperature can be estimated from MODIS LST and we conclude that MODIS LST could be used as a substitute for air temperature in other regions of the world where *in situ* data are rare. We demonstrate that it is possible to use calibration parameters derived using a very short observed daily time series and remotely sensed datasets to get an impression of the water cycle over a longer period.

We show that validation can be obtained by variable and scarce *in situ* data such as evaporation and gauge stations. We present that GRACE derived equivalent water thickness could be used to validate simulated water balance even in smaller catchments like Lake Manyara. The overall agreement between prediction and independent measurement from *in situ* and satellite observations confirm the validity of the annual water balance of Lake Manyara catchment obtained from the averaged monthly values. We suggest that, the changes in water balance including the dramatic rise in 2006–2007 are attributed to changes in climatic forcing parameters.

J2000g hydrological model reasonably captured the spatial and temporal variability of the water balance parameters in the catchment. Therefore, the model is suitable for hydrological modeling

in data scarce semi-arid basins due to its capability to incorporate both ground and remote sensing measurements.

The investigation presented herein is unique in three categories; first, we show the possibility of transferring parameters generated using a short time series data to calibrate a model with a long time series dataset. Second, we illustrate that evaporation data could be used to validate a model when runoff data is limited or unavailable. Third, we indicate that there is a great potential to make use of GRACE equivalent water thickness land mass grid datasets for hydrological studies even in smaller un-gauged lakes and basins in semi-arid environments. Based on our results we therefore conclude and propose that an estimation of water budget elements for a lake catchment in semi-arid regions worldwide with scarce existing data is possible using remote sensing approach.

To conclude, we point out and suggest that remote sensing based hydrological modeling is not aimed at replacing existing and more accurate techniques but to provide a robust tool to analyze and monitor areas where historical and *in situ* data are scarce. Most of the emerging countries lack the infrastructure that would permit accurate environmental monitoring. Our approach is not meant to deliver absolute values but to give the user a fairly robust estimation of the hydrological compartments and their temporal evolutions. This approach can have valuable applications for the monitoring of sensible water cycles and water resources in un-gauged remote areas.

Acknowledgments

We are indebted to the German Academic Exchange Service (DAAD) for supporting the PhD research project of the first author at the TU Bergakademie Freiberg, Germany. We would like to acknowledge the Tanzania Meteorological Agency for providing meteorological datasets and Langen R. M. Mallya for providing us with the lake Manyara's bathymetry data. We acknowledge the accessibility of GRACE land data. The data were processed by Sean Swenson and supported by the NASA MEASURES Program. We also express our gratitude to Adam Szulc for proofreading the manuscript.

References

1. Troch, P.A. Data Assimilation for Regional Water Balance Studies in Arid and Semi-arid Areas (Case Study: The Volta Basin Upstream the Akosombo Dam in Ghana). In Proceedings of the First MSG RAO Workshop, European Space Agency ESASP-452, Bologna, Italy, 17–19 May 2000; 2000CNR, Harris, R.A., Ed.; ESA: Bologna, Italy, 2000; p. 163.
2. Güntner, A.; Krol, M.S.; de Araújo, J.C.; Bronstert, A. Simple water balance modelling of surface reservoir systems in a large data-scarce semi-arid region. *Hydrol. Sci.* **2004**, *49*, 901–918.
3. Andersen, F.H. *Hydrological Modeling in a Semi-arid Area Using Remote Sensing Data*; University of Copenhagen: Copenhagen, Denmark, 2008.
4. Güntner, A.; Bronstert, A. Representation of landscape variability and lateral redistribution processes for large-scale hydrological modelling in semi-arid areas. *J. Hydrol.* **2004**, *267*, 136–161.
5. Yanda, P.Z.; Madulu., N.F. Water resource management and biodiversity conservation in the Eastern Rift Valley Lakes, Northern Tanzania. *Phys. Chem. Earth* **2005**, *30*, 717–725.

6. Böhme, B.; Steinbruch, F.; Gloaguen, R.; Heilmeier, H.; Merkel, B. Geomorphology, hydrology, and ecology of Lake Urema,central Mozambique, with focus on lake extent changes. *Phys. Chem. Earth* **2006**, *31*, 745–752.
7. Goerner, A.; Jolie, E.; Gloaguen, R. Non-climatic growth of the saline Lake Beseka, Main Ethiopian Rift. *J. Arid Environ.* **2008**, *73*, 287–295, ISSN 0140-1963.
8. Simonsson, L. *Applied Landscape Assessment in a Holistic Perspective, A Case Study from Babati District, North-central Tanzania*; Department of Earth Science, Uppsala University: Uppsala, Sweden, 2001.
9. Krause, P.; Hanisch, S. Simulation and analysis of the impact of projected climate change on the spatially distributed waterbalance in Thuringia, Germany. *Adv. Geosci.* **2009**, *21*, 33–48.
10. Milzow, C.; Krogh, P.E.; Bauer-Gottwein, P. Combining satellite radar altimetry, SAR surface soil moisture and GRACE total storage changes for hydrological model calibration in a large poorly gauged catchment. *Hydrol. Earth Syst. Sci.* **2011**, *15*, 1729–1743.
11. Khan, S.I.; Adhikari, P.; Hong, Y.; Vergara, H.; Adler, R.F.; Policelli, F.; Irwin, D.; Korme, T.; Okello, L. Hydroclimatology of Lake Victoria region using hydrologic model and satellite remote sensing data. *Hydrol. Earth Syst. Sci.* **2011**, *15*, 107–117.
12. Becker, M.; LLovel, W.; Cazenave, A.; Güntner, A.; Cretaux, J. Recent hydrological behavior of the East African great lakes region inferred from GRACE, satellite altimetry and rainfall observations. *Comptes Rendus Geosci.* **2010**, *342*, 223–233.
13. Hwang, C.; Kao, Y.; Tangdamrongsub, N. A preliminary analysis of lake level and water storage changes over lakes Baikal and Balkhash from satellite altimetry and gravimetry. *Terr. Atmos. Ocean. Sci.* **2011**, *22*, 97–108.
14. Swenson, S.C.; Wahr, J. Monitoring the water balance of Lake Victoria, East Africa, from space. *J. Hydrol.* **2009**, *370*, 163–176.
15. Santillan, J.; Makinano, M.; Paringit, E. Integrated landsat image analysis and hydrologic modeling to detect impacts of 25-year land-cover change on surface runoff in a philippine watershed. *Remote Sens.* **2011**, *3*, 1067–1087.
16. Awange, J.L.; Sharifi, M.; Ogonda, G.; Wickert, J.; Grafarend, E.W.; Omulo, M. The falling Lake Victoria water levels: GRACE, TRIMM and CHAMP satellite analysis of the lake basin. *Water Resour. Manag.* **2008**, *22*, 775–796.
17. Landerer, F.W.; Swenson, S.C. Accuracy of scaled GRACE terrestrial water storage estimates. *Water Resour. Res.* **2012**, *48*, W04531.
18. Casey, M.; Ebinger, C.; Keir, D.; Gloaguen, R.; Mohamed, F. Strain accommodation in transitional rifts: Extension by magma intrusion and faulting in Ethiopian Rift magmatic segments. *Geol. Soc. Spec. Publ.* **2006**, *259*, 143–163.
19. Keranen, K.; Klemperer, S.L.; Gloaguen, R. Three-dimensional seismic imaging of a protoridge axis in the Main Ethiopian rift. *Geology* **2004**, *32*, 949–952.
20. Kurz, T.; Gloaguen, R.; Ebinger, C.; Casey, M.; Abebe, B. Deformation distribution and type in the Main Ethiopian Rift (MER): A remote sensing study. *J. Afr. Earth Sci.* **2007**, *48*, 100–114.
21. Somi, E.J. Palaeoenvironmental Change in Central and Coastal Tanzania during the Upper Cenozoic. Ph.D. Thesis, University of Stockholm, Stockholm, Sweden, 1993.

22. Kaspar, F.; Cubasch, U.; Offenbach, G. Simulation of East African precipitation patterns with the regional climate model CLM. *Meteorol. Z.* **2008**, *17*, 511–517.
23. Reason, C.J.C. Sensitivity of the southern African circulation to dipole sea-surface temperature patterns in the South Indian Ocean. *Int. J. Climatol.* **2002**, *22*, 377–393.
24. Birkett, C.; Murtugudde, R.; Allan, T. Indian Ocean climate event brings floods to East Africa's lakes and the Sudd Marsh. *Geophys. Resour. Lett.* **1999**, *26*, 1031–1034.
25. Wheater, H.; Sorooshian, S.; Sharma, K.D. *Hydrological Modelling in Arid and Semi-Arid Areas*; Cambridge University Press: Cambridge, UK, 2007; p. 195.
26. Pilgrim, D.H.; Chapman, T.G.; Doran, D.G. Problems of rainfallrunoff modelling in arid and semiarid regions. *Hydrol. Sci.* **1988**, *33*, 379–400.
27. Copeland, S.R. Potential hominin plant foods in northern Tanzania: Semi-arid savannas *versus* savanna chimpanzee sites. *J. Hum. Evol.* **2009**, *57*, 365–378.
28. Prins, H.T.; Loth, P.E. Rainfall patterns as background to plant phenology in northern Tanzania. *J. Biogeogr.* **1988**, *15*, 451–463.
29. Loveland, T.R.; Belward, A.S. The IGBP-DIS global 1 km land cover data set, DISCover first results. *Int. J. Remote Sens.* **1997**, *18*, 3289–3295.
30. Rabus, B.; Eineder, M.; Roth, A.; Baler, R. The shuttle radar topography mission—A new class of digital elevation models acquired by spaceborne radar. *ISPRS J. Photogramm.* **2003**, *57*, 241–262.
31. Jarvis, A.; Reuter, H.I.; Nelson, A.; Guevara, E. *Hole-Filled SRTM for the Globe Version 4*; available from the CGIAR-CSI SRTM 90m Database. Available online: http://srtm.csi.cgiar.org (accessed on 5 June 2010).
32. Sorooshian, S.; Lawford, R.; Try, P.; Rossow, W.; Roads, J.; Polcher, J.; Sommeria, G.; Schiffer, R. Water and energy cycles: Investigating the links. *World Meteorol. Org. Bull.* **2005**, *54*, 58–64.
33. Gebremichael, M.; Over, T.M.; Krajewski, W.F. Comparison of the scaling characteristics of rainfall derived from spacebased and ground-based radar observations. *J. Hydrometeorol.* **2006**, *7*, 1277–1294.
34. Kummerow, C.; Barnes, W.; Kozu, T.; Shiue, J.; Simpson, J. The tropical rainfall measuring mission (TRMM) sensor package. *J. Atmos. Ocean. Technol.* **1998**, *15*, 809–817.
35. Andermann, C.; Bonnet, S.; Gloaguen, R. Evaluation of precipitation data sets along the Himalayan front. *Geochem. Geophys. Geosyst.* **2011**, *12*, doi: 10.1029/2011GC003513.
36. Huffman, G.J.; Adler, R.F.; Rudolf, B.; Schneider, U.; Keehn, P.R. Global precipitation estimates based on a technique for combining satellite-based estimates, rain-gauge analysis, and NWP model precipitation. *J. Clim.* **1995**, *8*, 1284–1295.
37. Adler, R.F.; Huffman, G.J.; Chang, A.; Ferraro, R.; Xie, P.; Janowiak, J.; Rudolf, B.; Schneider, U.; Curtis, S.; Bolvin, D.; Gruber, A.; Susskind, J.; Arkin, P.; Nelkin, E. The version 2 Global Precipitation Climatology Project (GPCP) monthly precipitation analysis (1979-Present). *J. Hydrometeorol.* **2003**, *4*, 1147–1166.
38. Prigent , C. Precipitation retrieval from space: An overview. *Comptes Rendus Geosci.* **2010**, *342*, 380–389.
39. Wan, Z. New refinements and validation of the MODIS Land-Surface Temperature/Emissivity products. *Remote Sens. Environ.* **2008**, *112*, 59–74.

40. Ruhoff, A.L.; Paz, A.R.; Collischonn; Aragao, L.E.O.C.; Rocha, H.R.; Malhi, Y.S. A MODIS-based energy balance to estimate evapotranspiration for clear-sky days in Brazilian tropical Savannas. *Remote Sens.* **2012**, *4*, 703–725.
41. Wan, Z.; Zhang, Y.; Zhang, Q.; Li, Z.-L. Quality assessment and validation of the MODIS land surface temperature. *Int. J. Remote Sens.* **2004**, *25*, 261–274.
42. Tapley, B.D.; Bettadpur, S.; Watkins, M.; Reigber, C.H. The gravity recovery and climate experiment: Mission overview and early results. *Geophys. Res. Lett.* **2004**, *31*, doi:10.1029/2004GL019920.
43. Wahr, J.; Molenaar, M.; Bryan, F. Time variability of the Earth's gravity field: Hydrological and oceanic effects and their possible detection using GRACE. *J. Geophys. Res.* **1998**, *103*, 30205–30229.
44. Wahr, J.; Swenson, S.; Zlotnicki, V.; Velicogna, I. Time-variable gravity from GRACE: First results. *Geophys. Res. Lett.* **2004**, *31*, doi: 10.1029/2004GL019779.
45. Swenson, S.; Wahr, J. Post-processing removal of correlated errors in GRACE data. *Geophys. Res. Lett.* **2006**, *33*, doi: 10.1029/2005GL025285.
46. Crétaux, J.; Birkett, C. Lake studies from satellite radar altimetry. *Comptes Rendus Geosci.* **2006**, *338*, 1098–1112.
47. FAO.; IIASA.; ISRIC.; ISSCAS.; JRC. *Harmonized World Soil Database (version 1.1)*; FAO: Rome, Italy and IIASA: Laxenburg, Austria, 2009.
48. Iqbal, M. *An Introduction to Solar Radiation*; Academic Press: New York, NY, USA, 1983.
49. Strugnell, N.C.; Lucht, W.; Schaaf, C. A global albedo data set derived from AVHRR data for use in climate simulations. *Geophys. Res. Lett.* **2001**, *28*, 191–194.
50. Chen, J.M.; Liu, J.; Cihlar, J.; Goulden, M.L. Daily canopy photosynthesis model through temporal and spatial scaling for remote sensing applications. *Ecol. Model.* **1999**, *124*, 99–119.
51. Lambin, E.F. Monitoring forest degradation in tropical regions by remote sensing: Some methodological issues. *Glob. Ecol. Biogeogr.* **1999**, *8*, 191–198.
52. Yucel, I. Effects of implementing MODIS land cover and albedo in MM5 at two contrasting US regions. *J. Hydrometeorol.* **2006**, *7*, 1043–1060.
53. Breuer, L.; Eckhardt, K.; Frede, H.G. Plant parameter values for models in temperate climates. *Ecol. Model.* **2003**, *169*, 237–293.
54. Ge, J.; Qi., J.; Lofgren, B.M.; Moore, N.; Torbick, N.; Olson, J.M. Impacts of land use/cover classification accuracy on regional climate simulations. *J. Geophys. Res.* **2007**, *112*, D05107, doi:05110.01029/02006JD007404.
55. Zeng, X. Global vegetation root distribution for land modeling, notes and correspondence. *J. Hydrometeorol.* **2001**, *2*, *525*–530.
56. Kralisch, S.; Krause, P. JAMS: A Framework for Natural Resource Model Development and Application. In Proceedings of the iEMSs Third Biennial Meeting of International Environmental Modelling and Software Society, Burlington, VM, USA, 9–13 July 2006.
57. Dingman, S.L. *Physical Hydrology*; Prentice Hall: Upper Saddle River, NJ, USA, 2002.
58. Thornthwaite, C. An approach toward a rational classification of climate. *Geogr. Rev.* **1948**, *38*, 55–94.
59. Willmott, C.J.; Rowe, C.M.; Mintz, Y. Climatology of the terrestrial seasonal water cycle. *Int. J. Clim.* **1985**, *5*, 589–606.

60. Cardille, J.; Coe, M.T.; Vano, J. Impacts of climate variation and catchment area on water balance and lake hydrologic type in groundwater-dominated systems: A generic lake model. *Earth Interact.* **2004**, *8*, 1–24.
61. Awulachew, S.B. Modelling natural conditions and impacts of consumptive water use and sedimentation of Lake Abaya and Lake Chamo, Ethiopia. *Lakes Reserv. Res. Manag.* **2006**, *11*, 73–82.
62. Wilcox, B.; Seyfried, M.; Breshears, D. The Water Balance on Rangelands. In *Encyclopedia of Water Science*; Marcel Dekker: New York, NY, USA, 2003; pp. 791–794.
63. Allen, R.G.; Pereira, L.S.; Raes, D.; Smith, M. *Crop Evapotranspiration: Guidelines for Computing Crop Water Requirements*; FAO Irrigation and Drainage Paper 56; Food and Agriculture Organization of the United Nations: Rome, Italy, 1998; p. 300.
64. Kebede, S.; Travia, Y.; Alemayehub, T.; Marca, V. Water balance of Lake Tana and its sensitivity to fluctuations in rainfall, Blue Nile basin, Ethiopia. *J. Hydrol.* **2006**, *316*, 233–247.
65. Penman, H.L. Natural evaporation from open water, bare soil and grass. *Proc. R. Soc. Lond.* **1948**, *193*, 120–145.
66. Jensen, M.E., Burman, R.D., Allen, R.G.E., Eds. *Evaporation and Irrigation Water Requirements*; ASCE Manuals and Reports on Engineering Practices No. 70; ASCE: New York, NY, USA, 1990; p. 360.
67. Liu, Y.B.; Batelaan, O.; de Smedt, F.; Poórová, J.; Velcická, L. Automated Calibration Applied to a GIS-based Flood Simulation Model Using PEST. In *Floods, from Defence to Management*; van Alphen, J., van Beek, E., Taal, M., Eds.; Taylor-Francis Group: London, UK, 2005; pp. 317–326.
68. Abram, N.J.; Gagan, M.K.; Liu, Z.; Hantoro, W.S.; McCulloch, M.T.; Suwargadi, B. Seasonal characteristics of the Indian Ocean Dipole during the Holocene epoch. *Nature* **2007**, *445*, 299–302.
69. Paeth, H.; Hense, A. On the linear response of tropical African climate to SST changes deduced from regional climate model simulations. *Theor. Appl. Clim.* **2006**, *83*, 1–19.
70. Evans, C.; Davies, T.D. Causes of concentration/discharge hysteresis and its potential as a tool for the analysis of episode hydrochemistry. *Water Resour. Res.* **1998**, *34*, 129–137.
71. Chanat, J.G.; Rice, K.C.; Hornberger, G.M. Consistency of patterns in concentration-discharge plots. *Water Resour. Res.* **2002**, *38*, 1147.
72. Andermann, C.; Longuevergne, L.; Bonnet, S.; Crave, A.; Philippe Davy, P.; Gloaguen, R. Impact of transient groundwater storage on the discharge of Himalayan rivers. *Nat. Geosci.* **2012**, *5*, 127–132.
73. Bouwer, H. Estimating and Enhancing Groundwater Recharge. In *Groundwater Recharge*; Sharma, M.L., Ed.; Balkema: Rotterdam, The Netherlands, 1989.
74. Krause, P.; Biskop, S.; Helmschrot, J.; Flugel, W.A.; Kang, S.; Gao, T. Hydrological system analysis and modelling of the Nam Co basin in Tibet. *Adv. Geosci.* **2010**, *27*, 29–36.
75. Bormann, H. Evaluation of hydrological models for scenario analyses: Signal-to-noise-ratio between scenario effects and model uncertainty. *Adv. Geosci.* **2005**, *5*, 43–48.
76. Frappart, F.; Papa, F.; Famiglietti, J.S.; Prigent, C.; Rossow, W.B.; Seyler, F. Interannual variations of river water storage from a multiple satellite approach: A case study for the Rio Negro River basin, Atmospheres. *J. Geophys. Res.* **2008**, *113*, D21104, doi:21110.21029/ 22007JD009438.

77. Calmant, S.; Seyler, F.; Cretaux, J. Monitoring continental surface waters by Satellite Altimetry. *Surv. Geophys.* **2008**, *29*, 247–269, doi: 210.1007/s10712-10008-19051-10711.
78. Mercier, F.; Cazenave, A.; Maheu, C. Interannual lake level fluctuations (1993–1999) in Africa from Topex/Poseidon: Connections with ocean-atmosphere interactions over the Indian Ocean. *Glob. Planet. Chang.* **2002**, *32*, 141–163.